

On the Interaction of Adaptive Population Control with Cumulative Step-Size Adaptation

Amir Omeradzic and Hans-Georg Beyer

Abstract—Three state-of-the-art adaptive population control strategies (PCS) are theoretically and empirically investigated for a multi-recombinative, cumulative step-size adaptation Evolution Strategy $(\mu/\mu_I, \lambda)$ -CSA-ES. First, scaling properties for the generation number and mutation strength rescaling are derived on the sphere in the limit of large population sizes. Then, the adaptation properties of three standard CSA-variants are studied as a function of the population size and dimensionality, and compared to the predicted scaling results. Thereafter, three PCS are implemented along the CSA-ES and studied on a test bed of sphere, random, and Rastrigin functions. The CSA-adaptation properties significantly influence the performance of the PCS, which is shown in more detail. Given the test bed, well-performing parameter sets (in terms of scaling, efficiency, and success rate) for both the CSA- and PCS-subroutines are identified.

Index Terms—Evolution Strategy, Population Size Adaptation, CSA-ES, Benchmark

I. INTRODUCTION

Evolution Strategies (ES) have shown to be well-suited for the optimization of test functions subjected to strong noise or high multimodality with adequate global structure. The crucial strategy parameter in both cases is the population size. On noisy functions, such as the noisy sphere, large populations enable to improve the signal-to-noise ratio of the ES and reduce the expected residual distance to the optimizer [1]. For well-structured highly multimodal problems, e.g., the Rastrigin function, they help to facilitate a global search, enabling to locate the global optimizer among exponentially many (in the dimensionality) local optima [2], [3]. While models for the population sizing for an multi-recombinative ES on the Rastrigin function are derived in [2], [3], the results of [4] demonstrate the importance of tuning the population size for the highest efficiency on Rastrigin.

Adaptive population control strategies (abbreviated as PCS) are able to adapt to both strong noise [5], [6], [7] and high multimodality [7], [8] by increasing the population size when insufficient algorithm performance is detected. While benchmarks on the well-known Black-Box Optimization Benchmarking (BBOB) test bed [9] are available in many cases, an in-depth analysis of adaptive population control is still pending. Furthermore, PCS are often tuned for the underlying test bed, such that direct comparison between different methods turns out to be difficult in some cases. In principle, adaptive

population control can be implemented into any ES. State-of-the-art ES use covariance matrix adaptation (CMA) [10] for the search space distribution together with cumulative step-size adaptation (CSA) [11], [12] for the global mutation strength. As it turns out, there is significant dependence of the PCS performance on the underlying CMA- and CSA-parametrization. This also holds among standard implementations of the CSA-ES, which will be shown. Population control cannot be studied isolated from the underlying mutation strength adaptation. A change of the population size usually results in changes of the mutation strength, which in turn influences the performance measure of the PCS. Hence, three state-of-the-art PCS routines [6], [7], [8] will be selected that are suitable for both noisy and multimodal problems. The PCS will incorporate performance measures both in search space and in fitness space, respectively. However, they will be investigated for isotropic mutations by using only the CSA-ES (without CMA) on a simple test bed. The idea is to reduce the problem complexity and provide theoretical reasoning for the parameter choices. Hence, adaptation time-scales and mutation strength rescaling are analyzed for CSA and PCS both theoretically and experimentally. The obtained parametrization is then applied to all PCS, enabling a direct comparison of the methods for the first time. Furthermore, the influence of different CSA-variants on adaptive population control is illustrated.

In the next Sec. II, the adaptive population control routine is introduced, which is later investigated in Sec. V. In Sec. III, preliminary theoretical results are derived which enable a better understanding the ES in the limit of large population sizes. In Sec. IV, a simple population change schedule is introduced to test the stability of the CSA. Then, the adaptive PCS are introduced and discussed in Sec. V. Furthermore, their performances are compared and the influence of the CSA is discussed. Finally, conclusions are drawn in Sec. VI.

II. CSA-ES WITH ADAPTIVE POPULATION CONTROL

The multi-recombinative $(\mu/\mu_I, \lambda)$ -CSA-ES with adaptive population control is given in Alg. 1. It operates with isotropic mutations of strength σ . At this point, the goal is to introduce the general algorithm, while the details of the respective population control subroutines are presented later in Alg. 2. The parent and offspring population is denoted by μ and λ , respectively, with the truncation ratio $\vartheta := \mu/\lambda$ ($\vartheta = 1/2$ will be used). The CSA-specific parameters (Lines 2, 7-17) are discussed in Sec. III. Generic (common) parameters of the PCS are initialized in Line 3 and specific parameters in Line 4. The PCS-methods to be used are based on [8] (APOP),

The authors are with the Research Center Business Informatics, Vorarlberg University of Applied Sciences, 6850 Dornbirn, Austria.

This research was funded by the Austrian Science Fund (FWF) under grant P33702-N.

This work is licensed under a Creative Commons Attribution 4.0 License.

[6] (pcCSA), and [7] (PSA). Each method measures the ES-performance (denoted by \mathcal{P}) by its own means (see Sec. V). Lines 21-29 control which single PCS is used throughout an optimization. The population is changed within the bounds $[\mu_{\min}, \mu_{\max}]$ via a factor $\alpha_\mu > 1$ using a simple schedule (Lines 31-37). A generational idle (wait) time $\Delta_g > 0$ can be set (Line 5). Rescaling of the mutation strength is performed in Line 41 and will be discussed in Sec. III. The algorithms are later tested on a set of test functions.

III. THE CSA-ES FOR LARGE POPULATION SIZES

A. Scaling of Generation Number and Mutation Strength

In this section, important theoretical and experimental results regarding the scaling behavior of the CSA-ES in the limit of large population sizes are shown on the sphere function $f(R) = R^2$, $R = \|\mathbf{y}\|$, $\mathbf{y} \in \mathbb{R}^N$. It will be shown that different standard CSA-implementations have different adaptation properties w.r.t. the population size μ and dimensionality N . These results will enable to derive a generation number scaling for the ES in the limit of large μ to achieve a given (relative) target. The results will illustrate why large differences in the generation number are observed for the standard CSA-implementations. These results will also be relevant for adaptive population control in Sec. V, showing notable differences of the performance depending on the chosen CSA and its adaptation properties.

The subsequent derivation of the generation number as a function of the progress rate was already given in [13, Sec. 2.4]. The progress rate φ is defined as the expected residual distance change between two generations g and $g+1$ as

$$\varphi^{(g)} := R^{(g)} - \mathbb{E} \left[R^{(g+1)} \right]. \quad (1)$$

Due to the scale-invariance of the sphere, one can define the normalized quantities (denoted by $*$) as

$$\varphi^* = \varphi N / R, \quad \sigma^* = \sigma N / R. \quad (2)$$

A properly working σ -adaptation, such as the CSA, attains constant σ^* and φ^* (in expectation) on the sphere, giving linear convergence order [13]. Assuming constant φ^* , one can derive the generation number $G := g - g_0$ for a given relative change $R^{(g)}/R^{(g_0)}$ under the assumption $\varphi^*/N \ll 1$ as [13, (2.105)]

$$G = (N/\varphi^*) \ln \left(R^{(g_0)}/R^{(g)} \right). \quad (3)$$

The next step is to derive φ^* for large populations. One can start with the (normalized) progress rate of the sphere derived in [13, (6.54)] with progress coefficient $c_{\mu/\mu, \lambda}$

$$\varphi^* = \frac{c_{\mu/\mu, \lambda} \sigma^* (1 + \sigma^{*2}/2\mu N)}{\sqrt{1 + \sigma^{*2}/\mu N} \sqrt{1 + \sigma^{*2}/2N}} - N \left(\sqrt{1 + \sigma^{*2}/\mu N} - 1 \right) + O \left(N^{-1/2} \right). \quad (4)$$

Progress rate (4) is visualized in Fig. 1. Note that there is a range $\sigma^* \in (0, \sigma_{\varphi_0}^*)$ where $\varphi^* > 0$. We will denote $\sigma_{\varphi_0}^*$ as the analytic second zero (being an approximation to be derived), while σ_0^* is the numerically obtained zero. Expression (4) needs to be simplified to enable closed-form

Algorithm 1 Population Size Control via $(\mu/\mu_I, \lambda)$ -CSA-ES

```

1:  $g \leftarrow 0$ 
2: initialize_CSA( $\mathbf{y}^{(0)}, \mathbf{s}^{(0)}, \sigma^{(0)}, c_\sigma, d_\sigma, D, E_\chi$ )
3: initialize_PCS_generic( $\mu^{(0)}, \mu_{\min}, \mu_{\max}, \vartheta, \alpha_\mu, \Delta_g$ )
4: initialize_PCS_specific( $\beta, L, f_{\text{rec}}^{(0)}, f_{\text{med}}^{(0)}, \mathbf{p}_m^{(0)}, \mathbf{p}_c^{(0)}$ )
5:  $w \leftarrow \Delta_g$ 
6: repeat

```

Standard $(\mu/\mu_I, \lambda)$ -CSA-ES

```

7:   for  $l = 1, \dots, \lambda$  do
8:      $\tilde{\mathbf{z}}_l \leftarrow [\mathcal{N}(0, 1), \dots, \mathcal{N}(0, 1)]$ 
9:      $\tilde{\mathbf{y}}_l \leftarrow \mathbf{y}^{(g)} + \sigma^{(g)} \tilde{\mathbf{z}}_l$ 
10:     $\tilde{f}_l \leftarrow f(\tilde{\mathbf{y}}_l)$ 
11:    end for
12:     $(\tilde{f}_{1;\lambda}, \dots, \tilde{f}_{m;\lambda}, \dots, \tilde{f}_{\mu;\lambda}) \leftarrow \text{sort}(\tilde{f}_1, \dots, \tilde{f}_\lambda)$ 
13:     $\mathbf{y}^{(g+1)} \leftarrow \frac{1}{\mu} \sum_{m=1}^{\mu} \tilde{\mathbf{y}}_{m;\lambda}$ 
14:     $\langle \mathbf{z} \rangle^{(g+1)} \leftarrow \frac{1}{\mu} \sum_{m=1}^{\mu} \mathbf{z}_{m;\lambda}$ 
15:     $\mathbf{s}^{(g+1)} \leftarrow (1 - c_\sigma) \mathbf{s}^{(g)} + \sqrt{\mu^{(g)} c_\sigma (2 - c_\sigma)} \langle \mathbf{z} \rangle^{(g+1)}$ 
16:    CSA (15):  $\sigma^{(g+1)} \leftarrow \sigma^{(g)} \exp \left[ \frac{1}{D} \left( \|\mathbf{s}^{(g+1)}\| / E_\chi - 1 \right) \right]$ 
17:    CSA (16):  $\sigma^{(g+1)} \leftarrow \sigma^{(g)} \exp \left[ \frac{c_\sigma}{d_\sigma} \left( \|\mathbf{s}^{(g+1)}\| / E_\chi - 1 \right) \right]$ 

```

Population Control Strategy (PCS)

```

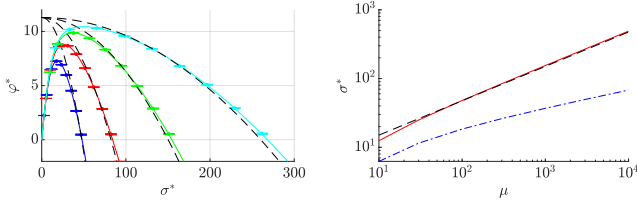
18:    $f_{\text{rec}}^{(g+1)} \leftarrow f(\mathbf{y}^{(g+1)})$ 
19:    $f_{\text{med}}^{(g+1)} \leftarrow \text{median}(\tilde{f}_{1;\lambda}, \dots, \tilde{f}_{m;\lambda}, \dots, \tilde{f}_{\mu;\lambda})$ 
20:    $g_0 \leftarrow g - L + 1$ 
21:   if PCS = APOP and  $g_0 \geq 0$  then
22:      $\mathcal{P} \leftarrow \text{get\_apop}()$ 
23:   else if PCS = pcCSA and  $g_0 \geq 0$  then
24:      $\mathcal{P} \leftarrow \text{get\_pccsa}()$ 
25:   else if PCS = PSA then
26:      $\mathcal{P} \leftarrow \text{get\_psa}()$ 
27:   else
28:      $\mathcal{P} \leftarrow 0$ 
29:   end if
30:   if  $w = 0$  then
31:     if  $\mathcal{P} < 0$  then
32:        $\mu^{(g+1)} \leftarrow \lceil \alpha_\mu \mu^{(g)} \rceil$ 
33:     else if  $\mathcal{P} > 0$  then
34:        $\mu^{(g+1)} \leftarrow \lfloor \mu^{(g)} / \alpha_\mu \rfloor$ 
35:     else
36:        $\mu^{(g+1)} \leftarrow \mu^{(g)}$ 
37:     end if
38:     if  $\mu^{(g)} \neq \mu^{(g+1)}$  then
39:        $\mu^{(g+1)} \leftarrow \min \left( \max(\mu^{(g+1)}, \mu_{\min}), \mu_{\max} \right)$ 
40:        $w \leftarrow \Delta_g$ 
41:        $\sigma^{(g+1)} \leftarrow \sigma^{(g)} r_\sigma(\mu^{(g)}, \mu^{(g+1)})$ 
42:        $\mu \leftarrow \mu^{(g+1)}, \lambda \leftarrow \text{round}(\mu^{(g+1)} / \vartheta)$ 
43:        $c_\sigma \leftarrow c_\sigma(\mu), D \leftarrow D(\mu), d_\sigma \leftarrow d_\sigma(\mu)$ 
44:     end if
45:   else
46:      $w \leftarrow w - 1$ 
47:   end if
48:    $g \leftarrow g + 1$ 
49: until termination criterion

```

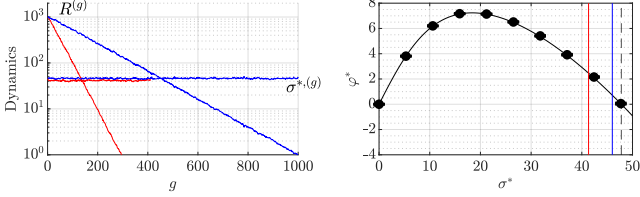
solutions. For large populations, one assumes $\mu N \gg \sigma^{*2}$ and $c_{\mu/\mu, \lambda} \simeq c_\vartheta$ is only a function of the truncation ratio ϑ [13, (6.113)]. Taylor-expansion in (4) yields $\sqrt{1 + \sigma^{*2}/\mu N} = 1 + \sigma^{*2}/2\mu N + O((\sigma^{*2}/\mu N)^2)$. Neglecting higher order terms, one gets a simplified expression

$$\varphi^* \simeq c_\vartheta \sigma^* / \sqrt{1 + \sigma^{*2}/2N} - \sigma^{*2}/2\mu. \quad (5)$$

Intermediate result (5) needs to be approximated further. As will be shown in Sec. II, the CSA-variants operate relatively



(a) On the left, $\varphi^*(\sigma^*)$ at $N = 100$ for $\mu = 100, 300, 1000, 3000$ and $\mu/\lambda = 1/2$ are shown. The solid lines show (4) and the corresponding data points (1) averaged over 10^4 trials and normalized using $\varphi^* = \varphi N/R$. The dashed line shows (6). On the right, (4) is used to numerically calculate the second zero σ_0^* (red solid) and $\hat{\sigma}^* = \arg \max \varphi^*(\sigma^*)$ (dash-dotted blue). The black dashed line shows approximation (7).



(b) On the left, median dynamics of (100/100_I, 200)-CSA-ES for $N = 100$ is shown (10 trials) using (17a) (red) and (17b) (blue). On the right, $\varphi^*(\sigma^*)$ is shown (data points: simulated; black curve: (4)). Furthermore, the vertical lines mark measured median values from the left with $\sigma_{ss}^* \approx 41.3$ ((17a), red, $\gamma \approx 0.86$), $\sigma_{ss}^* \approx 46.0$ ((17b), blue, $\gamma \approx 0.96$), and numerically obtained $\sigma_0^* \approx 47.8$ (dashed black).

Fig. 1: Progress rate φ^* and scale-invariant σ^* on the sphere.

slowly, i.e., closer to $\sigma_{\varphi_0}^*$ than to $\sigma^* = 0$. Slow adaptation decreases σ more slowly than fast adaptation while R is decreased. On the sphere, σ^* remains constant, such that slow adaptation yields a higher σ^* -level via (2). Furthermore, large populations attain higher σ^* -values due to recombination. Hence, we simplify (5) by assuming $\sigma^{*2}/2N \gg 1$, such that “1” is neglected within the square-root. One gets

$$\varphi^* \simeq \sqrt{2N}c_{\vartheta} - \sigma^{*2}/2\mu. \quad (6)$$

The zero of approximation (6) is easily obtained as

$$\sigma_{\varphi_0}^* \simeq (8N)^{1/4}(c_{\vartheta}\mu)^{1/2}. \quad (7)$$

Figure 1a shows (4) and (6) (left) and the second zero $\sigma_{\varphi_0}^*$ (right). One observes excellent agreement of (4) with one-generation experiments of (1). Furthermore, approximation (6) improves with increasing μ (and N), which was expected from the underlying assumptions. For (7) one observes good agreement of $\sigma_{\varphi_0}^*$ with σ_0^* for increasing μ . In Fig. 1a, note that the optimal $\hat{\sigma}^*$ decreases in relation to $\sigma_{\varphi_0}^*$ for fixed N with increasing μ . Using PCS on highly multimodal functions (with adequate global structure), small mutation strengths are undesirable since they increase the probability of local convergence. Hence, the approach is to characterize the CSA-adaptation on the sphere in terms of a steady-state σ_{ss}^* w.r.t. the second zero $\sigma_{\varphi_0}^*$ and not w.r.t. the optimal value. This will also be justified by the experiments of standard CSA implementations. Introducing a scaling factor $0 < \gamma < 1$ (slow-adaptation: $\gamma \lesssim 1$), one sets

$$\sigma_{ss}^* = \gamma \sigma_{\varphi_0}^* = \gamma(8N)^{1/4}(c_{\vartheta}\mu)^{1/2}. \quad (8)$$

Depending on the CSA parametrization (cumulation constant, damping), population size, and N , the ES achieves a steady-state σ_{ss}^* w.r.t. $\sigma_{\varphi_0}^*$ according to a ratio $\gamma = \sigma_{ss}^*/\sigma_{\varphi_0}^*$. An example of measured values is shown in Fig. 1b. Depending on the chosen CSA, one observes different measured $\gamma = \sigma_{ss}^*/\sigma_{\varphi_0}^*$. The limit $\gamma \rightarrow 1$ corresponds to vanishing progress (stagnation) on the sphere. The adaptation speed of the CSA will be characterized in terms of γ . Assuming the CSA attains a constant γ , (8) is inserted into (6), which is in turn used in (3). The progress rate yields

$$\varphi^* \simeq c_{\vartheta}(2N)^{1/2}(1 - \gamma^2). \quad (9)$$

After inserting (9) into (3), one obtains for $G = g - g_0$

$$G \simeq \sqrt{N} \frac{\ln(R^{(g_0)}/R^{(g)})}{\sqrt{2}c_{\vartheta}(1 - \gamma^2)}. \quad (10)$$

For constant γ and sufficiently large μ , the generation number scales independent of μ with \sqrt{N} (given a relative change of R). This is a remarkable result which is tested later in experiments. It is also useful when defining a time scale for the adaptation of PCS in Secs. IV and V.

Various PCS employ additional corrections of σ after μ has been changed between two generations [7], [8]. The idea is referred to as σ -rescaling and should accelerate the σ -adaptation further. However, this has effects on the stability of the CSA (see Sec. IV). Given the results on the sphere in (8) with $\sigma^* = \sigma N/R$, we derive a $\sqrt{\mu}$ -law for the σ -rescaling $r_{\sigma} := \sigma^{(g+1)}/\sigma^{(g)}$ (Alg. 1, Line 41). Since the distance to the optimizer does not change during σ -rescaling, one has $R^{(g+1)} = R^{(g)}$. From (8) one sees that $\sigma^{(g)} = \sigma_{ss}^{*(g)} R^{(g)}/N = K\sqrt{\mu^{(g)}}R^{(g)}/N$ and $\sigma^{(g+1)} = \sigma_{ss}^{*(g+1)} R^{(g+1)}/N = K\sqrt{\mu^{(g+1)}}R^{(g+1)}/N$ (constant $K > 0$). Thus, one gets $r_{\sigma} = \sqrt{\mu^{(g+1)}/\mu^{(g)}}$ and finally

$$\sigma^{(g+1)} = \sigma^{(g)} \sqrt{\mu^{(g+1)}/\mu^{(g)}}. \quad (11)$$

Alternatively, in the case of $N \rightarrow \infty$ and $\mu \ll N$, (4) can be used to derive the well-known progress rate

$$\varphi^* = c_{\mu/\mu, \lambda} \sigma^* - \sigma^{*2}/2\mu. \quad (12)$$

In this case, the optimal value (maximizer) and the second zero of (12) are $\hat{\sigma}^* = c_{\mu/\mu, \lambda} \mu$ and $\sigma_{\varphi_0}^* = 2c_{\mu/\mu, \lambda} \mu$. Based on these results, one obtains mutatis mutandis a linear scaling law for the σ -rescaling as

$$\sigma^{(g+1)} = \sigma^{(g)} \mu^{(g+1)}/\mu^{(g)}. \quad (13)$$

While (13) is not expected to yield better results (since $\mu \ll N$), it will still be tested as it was used in [7] (see supplementary material A-A for a derivation on the sphere).

B. Analysis of the CSA-ES

In this section, the adaptation properties of the CSA-ES are studied. The goal is to first investigate $\gamma = \gamma(\mu, N)$ from (8) and later apply the results to obtain $G = G(\mu, N)$ from (10). The CSA-ES has already been investigated in [14] for three standard CSA-parametrizations. Hence, only the main results will be stated and more details are found in [14]. The

cumulation path \mathbf{s} of the CSA-adaptation is given in terms of cumulation constant c_σ and recombined mutation direction $\langle \mathbf{z} \rangle$

$$\mathbf{s}^{(g+1)} = (1 - c_\sigma)\mathbf{s}^{(g)} + \sqrt{c_\sigma(2 - c_\sigma)}\mu\langle \mathbf{z} \rangle^{(g+1)}. \quad (14)$$

Then, the path length $\|\mathbf{s}^{(g+1)}\|$ is measured and compared to its expected result under random selection. The first update rule for the σ -change is chosen according to [15]

$$\sigma^{(g+1)} = \sigma^{(g)} \exp \left[\frac{1}{D} \left(\left\| \mathbf{s}^{(g+1)} \right\| / E_\chi - 1 \right) \right], \quad (15)$$

where D is a damping factor. Alternatively, a slightly different update rule [10, (44)] with damping d_σ yields

$$\sigma^{(g+1)} = \sigma^{(g)} \exp \left[\frac{c_\sigma}{d_\sigma} \left(\left\| \mathbf{s}^{(g+1)} \right\| / E_\chi - 1 \right) \right], \quad (16)$$

which is often chosen in recent implementations of the CSA. E_χ is the expected value of a chi-distributed random variate $\chi \sim \|\mathcal{N}(\mathbf{0}, \mathbf{1})\|$. One usually uses the approximation $E_\chi \simeq \sqrt{N}(1 - 1/4N + 1/21N^2)$ for large N . The CSA variants under investigation are parameterized as

$$\text{Eq. (15) with } c_\sigma = 1/\sqrt{N}, \quad D = c_\sigma^{-1}. \quad (17a)$$

$$\text{Eq. (15) with } c_\sigma = 1/N, \quad D = c_\sigma^{-1} \quad (17b)$$

$$\text{Eq. (16) with } c_\sigma = \frac{\mu + 2}{N + \mu + 5}, \quad \text{and} \quad (17c)$$

$$d_\sigma = 1 + c_\sigma + 2 \max \left(0, \sqrt{(\mu - 1)/(N + 1)} - 1 \right).$$

CSA implementations (17a) and (17b) were investigated in more detail in [11], [15]. [15] derives the inverse proportionality $D = c_\sigma^{-1}$ with $c_\sigma = N^{-a}$ for $\frac{1}{2} \leq a \leq 1$ based on theoretical and experimental investigations on the sphere ($\mu \ll N$, see also (12)). CSA (17c) is a newer implementation that is part of the default CMA-ES, see also [10] (μ_{eff} due to weighted recombination was replaced by μ).

As a first step, basic adaptation properties of the three variants are identified. Note that c_σ and D of (17a) and (17b) are independent of μ . Changing the population size should not have large influence on the adaptation characteristics. For (17c), c_σ and d_σ requires further analysis under the assumption $\mu \gg N$. c_σ yields simply

$$c_\sigma = \frac{\mu(1 + 2/\mu)}{\mu(1 + N/\mu + 5/\mu)} \stackrel{\mu \rightarrow \infty}{\simeq} 1. \quad (18)$$

The cumulation time parameter c_σ approaches ‘‘1’’ as μ is increased, which results in a faster cumulation in (14). Now the factor c_σ/d_σ is brought into a similar form as $1/D$ in (15). One finds in [14] that c_σ/d_σ yields a damping factor $D = 1 + 1/c_\sigma + g(N, \mu)/c_\sigma$ with $g(N, \mu) := 2 \max \left(0, \sqrt{\frac{\mu-1}{N+1}} - 1 \right)$. Hence, the damping term $g(N, \mu)/c_\sigma$ yields the scaling

$$g(N, \mu)/c_\sigma \simeq 2\sqrt{\mu/N} \quad (\mu \rightarrow \infty). \quad (19)$$

The resulting damping D of (17c) scales with $\sqrt{\mu}$ according to (19) for fixed N and c_σ approaches one with (18). Hence, CSA (17c) employs a μ -dependent damping which is in contrast to (17a) and (17b). If μ is changed during adaptive population control, the CSA adaptation characteristic in terms of γ will be affected, which is shown later in Fig. 2. In [14] the three

CSA-implementations are investigated and the CSA update equations are expressed in the sphere steady-state, where the scale-invariant mutation strength σ^* and progress rate φ^* are constant in expectation (see also Fig. 1b). By applying certain approximations (assuming sufficiently slow progress $\varphi^*/N \ll 1$ and large dimensionality N), this approach allows for closed-form of the CSA sphere steady-state as a function of the given cumulation constant and damping. By including this dependency into a single constant b [14, (58)]

$$b := \left(c_\sigma D / (1 - c_\sigma) + \sqrt{2} c_\sigma D / \sqrt{N} \right)^{-1}, \quad (20)$$

one can derive the respective γ from (8) as a function of b (assuming $1/\sqrt{2} < \gamma < 1$) as [14, (57)]

$$\gamma = \sqrt{\frac{1}{2} \left(\sqrt{1 + b^2} - b + 1 \right)}. \quad (21)$$

The result (21) is interesting as it relates the CSA-parameters and N to a scale factor γ on the left side. Demanding γ to be constant and independent of μ and N , one must choose $D \propto \sqrt{N}$ and $c_\sigma = D^{-1}$ within b (this holds with $O(1/\sqrt{N})$). This is only fulfilled by CSA (17a). In this case, the analytic solution of $\gamma \approx 0.90$ ($\mu/\lambda = 1/2$) was derived as an approximation [14, (63)]. For (17b) one has $D \propto N$, and for (17c) $D \propto \sqrt{\mu/N}$ via (19). The limit $D \rightarrow \infty$ ($0 < c_\sigma < 1$) yields $b \rightarrow 0$ and $\gamma \rightarrow 1$. In this limit, $\sigma_{\text{ss}}^* \rightarrow \sigma_{\varphi_0}^*$ in (8) and the progress rate vanishes $\varphi^* \rightarrow 0$ by approaching its second zero. Hence, (17b) becomes increasingly slow for large N , while (17c) becomes slower for increasing ratio $\sqrt{\mu/N}$.

In Fig. 2, experiments on the sphere are shown to compare the CSA-variants with the predicted adaptation behavior in terms of γ . To this end, the dimensionality N and population size μ are varied. The measured steady-state σ_{ss}^* is averaged over at least 10 trials and the median is taken over the measured $\sigma^{*(g)}$ (the median is necessary due to a slightly skewed distribution of σ^* at small N). The measured σ_{ss}^* is normalized by σ_0^* (numerically obtained second zero of (4)¹), yielding a reference value for γ . In Figs. 2a and 2b, the measured ratio remains relatively constant for sufficiently large μ for (17a) and (17b). CSA (17c) shows a significant increase of γ as μ increases, which was expected from its damping D . Deviations between the predicted γ (dashed) and measurement (solid) are expected to occur due to the underlying (necessary) approximations applied in [14]. In Fig. 2c, the dimensionality is varied. CSA (17a) remains relatively constant, while γ of (17b) increases for larger N , which was expected from its damping $D \propto N$. CSA (17c) shows a decreasing γ due to $D \propto \sqrt{\mu/N}$. In Fig. 2d, both μ and N are varied together by maintaining $\mu = 2N$. CSA (17a) and (17c) remain approximately constant, while for (17b) $\gamma \rightarrow 1$. As expected, only (17a) maintains an approximately constant ratio (best agreement for large N and $\mu \gg N$) at $\gamma \lesssim 0.9$, which agrees satisfactory with the prediction (21). Furthermore, it realizes lower γ -levels, which leads to higher progress rates φ^*

¹For $N \gtrsim 100$ one may numerically calculate σ_0^* using (4). For $N < 100$, the progress rate zero is calculated from one-generation experiments of (1) to have a higher accuracy. Slow adaptation yields σ^* very close to σ_0^* such that the accuracy of (4) is reduced due to missing $O(N^{-1/2})$ -terms.

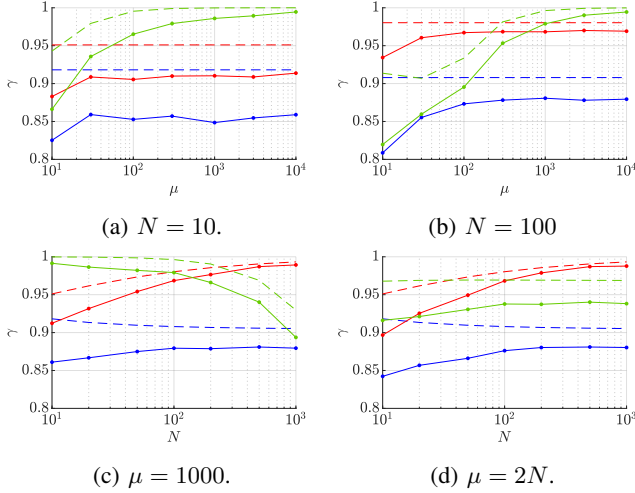


Fig. 2: Steady-state ratio γ on the sphere function for $\vartheta = 1/2$. Measured ratio σ_{ss}^*/σ_0^* (solid, with dots) compared to γ from (21) (dashed) for the CSA variants (17a) (blue), (17b) (red), and (17c) (green).

(cf. Fig. 1b). Note that all three CSA yield relatively large γ -values between 0.8 and 1. This means they achieve comparably low progress rates, which holds especially when compared to a self-adaptive ES ($\gamma \gtrsim 0.6$, see [14]). However, on highly multimodal problem instances, slower adaptation is beneficial to achieve higher success rates [2], [4].

Now that the results for γ have been investigated in Fig. 2, one can study the generation number G from (10). Figure 3 shows G evaluated at constant μ (left) and constant N (right). CSA (17a) yields very good agreement with (10) due to the relatively constant γ . On the left, one observes a \sqrt{N} -law for G . On the right, G remains asymptotically constant for increasing μ . CSA (17b) shows a faster increase of G than \sqrt{N} (left), which can be attributed to the increased damping ($\gamma \rightarrow 1$) at large N . On the right, it also remains asymptotically constant for large μ , requiring more generations due to slower adaptation. CSA (17c) shows a different characteristic, being comparably slow at high ratios μ/N and fast at low ratios mostly due to its damping D . The G -asymptotic for $\mu \rightarrow \infty$ is a notable result. From a modeling perspective, one could argue that CSA (17a) shows important (desired) properties for PCS on sphere-like functions. The adaptation is comparably fast and one observes a generational speedup of G as μ is increased from small initial values. At large μ , asymptotic behavior is observed. CSA (17c) slows down its adaptation as μ is increased, which can be detrimental in terms of efficiency (see later discussion of Fig. 9).

IV. POPULATION CONTROL SCHEDULE

Before adaptive population control is investigated further, the CSA-stability w.r.t. changes of μ is investigated. The PCS will later introduce additional method-specific feedback in the ES-dynamics. Having effects of σ - and μ -adaptation combined makes the analysis more difficult. Hence, we introduce a simple $\mu^{(g)}$ -schedule on the sphere function, generating artificial μ -changes. The schedule is defined as being constant

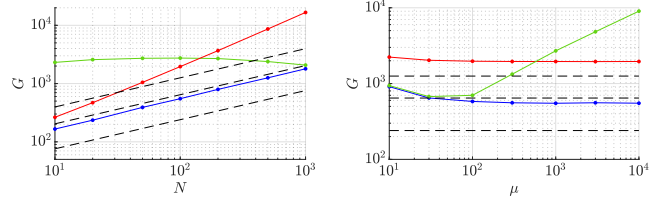


Fig. 3: Number of generations G , see (10), to reach the target $R^{(g)}/R^{(g_0)} = 10^{-6}$ using a (1000/1000_I, 2000)-ES (left) and $N = 100$ (right). The average over 10 runs is taken. The solid lines show (17a) in blue, (17b) in red, and (17c) in green. G from (10) at $\gamma = 0.9$ is displayed in dash-dotted black. The lower and upper dashed lines show $\gamma = 0.8, 0.95$, respectively.

within the first 200 generations. Then, μ is increased using a factor α_μ as $\mu^{(g+1)} = \lceil \mu^{(g)} \alpha_\mu \rceil$ until μ_{\max} is reached. After reaching μ_{\max} , it is decreased as $\mu^{(g+1)} = \lfloor \mu^{(g)} / \alpha_\mu \rfloor$ until $\mu^{(0)}$ is reached. This oscillation is repeated multiple times to check the stability. Furthermore, the effect of rescaling σ (via $\sigma^{(g+1)} = r_\sigma \sigma^{(g)}$) on the stability of the CSA is tested. Given results (11) and (13), one can summarize the three tested rescaling methods as

$$r_\sigma = 1 \quad (\text{no rescaling}) \quad (22a)$$

$$r_\sigma = (\mu^{(g+1)}/\mu^{(g)})^{1/2} \quad (22b)$$

$$r_\sigma = \mu^{(g+1)}/\mu^{(g)}. \quad (22c)$$

The experiments in Figs. 4a and 4b show the convergence dynamics on the sphere function. Two different values for N are tested based on Fig. 2, where large differences for $\gamma(N)$ could be observed. In both experiments, $\alpha_\mu = 2$ is chosen with $\mu^{(0)} = \mu_{\min} = 4$ and $\mu_{\max} = 1024$. The dynamics are initialized at $s^{(0)} = \mathbf{1}$ and $\sigma^{(0)} = \sigma_{\varphi_0}^* R/N$ using (7), which reduces undesired initialization effects. In Fig. 4b, a waiting time $\Delta_g = \lceil \sqrt{N} \rceil$ is applied after a population change based on the result $G \propto \sqrt{N}$ from (10). This introduces more time for the CSA to adapt to the μ -change. Note that no waiting is implemented in Fig. 4a.

In Fig. 4a, one observes that no rescaling ($r_\sigma = 1$) leads to instabilities (divergence) of the CSA in most cases, while $r_\sigma = (\mu^{(g+1)}/\mu^{(g)})^{1/2}$ shows very good results in terms of convergence speed for all configurations. It also shows the least amount of $R^{(g)}$ -oscillations along its convergence. Scaling $r_\sigma = \mu^{(g+1)}/\mu^{(g)}$ shows mixed results. It helps to stabilize the CSA in some cases. However, it would be more suitable for μ -control with $\mu \ll N$ due to progress rate (12). The instabilities are related to the CSA cumulation constant c_σ , the damping D , and the applied r_σ . Due to the high rate of change of μ , the CSA is constantly adapting to the changing population. In the worst case, one observes divergence due to σ^* being outside the positive progress range $\sigma^* \in (0, \sigma_{\varphi_0}^*)$, see Fig. 1b. Note that CSA (17a) (first row) shows consistent results as N is increased. On the other hand, CSA (17c) converges with $r_\sigma = 1$ due to the higher damping at small $N = 10$ (although with large oscillations of R), but diverges due to lower damping at large $N = 1000$. In Fig. 4b, the waiting time $\Delta_g = \lceil \sqrt{N} \rceil$ yields more time for the CSA to

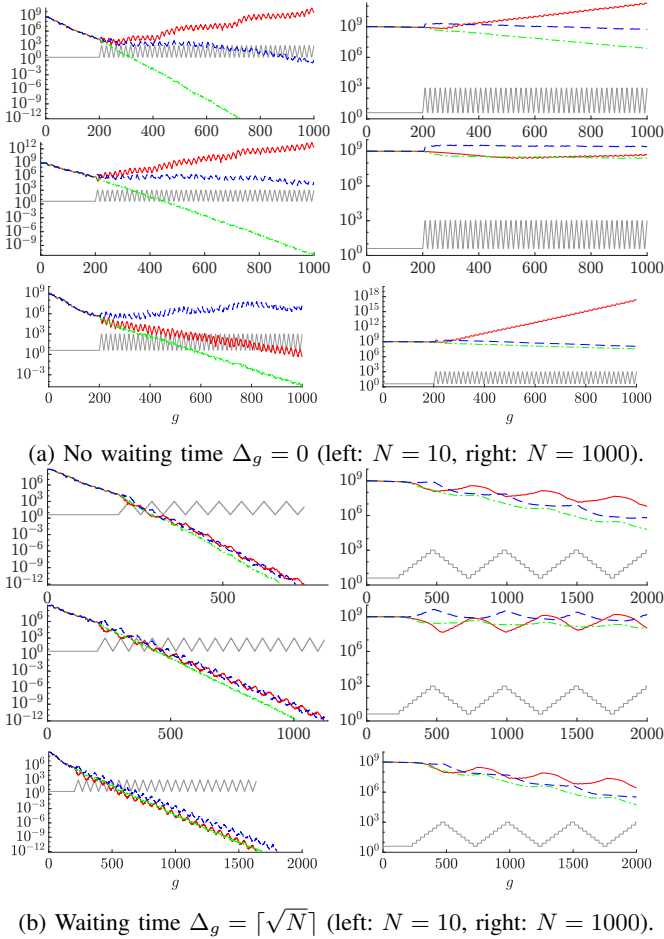


Fig. 4: Stability of CSA on the sphere using predefined $\mu^{(g)}$ -schedule. The gray lines show $\mu^{(g)}$ and the colored lines the $R^{(g)}$ -dynamics of (22a) (red), (22b) (green), and (22c) (blue). The tested CSAs are (17a), (17b), and (17c), from top to bottom, respectively for (a) and (b).

adapt to the current population size $\mu^{(g)}$. Again, (22b) shows the most stable results. As expected, $\Delta_g > 0$ stabilizes all the CSA variants and for all r_σ -choices. The obtained results show that (22b) is the preferred rescaling of σ on the sphere in terms of stability. In Sec. V it will be shown that certain PCS are more sensitive to changes of σ than others. The influence of r_σ with active PCS will also be studied.

V. ADAPTIVE POPULATION CONTROL STRATEGIES

For the subsequent investigations, three state-of-the-art PCS are implemented based on [8] (APOP), [6] (pcCMSA), and [7] (PSA). These algorithms were designed and tested for adaptive population control on ES for a broader range of functions (noisy and/or multimodal, details below). As for the analysis, the idea is to implement simplified versions of the PCS. Hence, only the performance measuring routines are implemented. Note that the population control subroutines of Alg. 1 are given in Alg. 2, including the pseudocode for APOP, pcCMSA, and PSA. A simple routine for the change of μ is realized according to Alg. 1 (Lines 31-37). We omit the introduction of additional damping parameters for the $\mu^{(g)}$ -change (as done in

[7], [8], analogous to D in (15)) since it adds more complexity. Furthermore, (22b) is used for the σ -rescaling on all methods.

The APOP was introduced in [8] for the CMA-ES and tested on a larger set of noiseless functions. The basic idea is to count the number of (median-)fitness deteriorations within the last L generations (in [8] they use a fixed length $L = 5$). Defining the median over selected f -values as $f_{\text{med}}^{(g)} := \text{median}(f_{m;\lambda}^{(g)})$, $m = 1, \dots, \mu$, the difference is given by

$$\Delta f^{(g)} = f_{\text{med}}^{(g)} - f_{\text{med}}^{(g-1)}. \quad (23)$$

Then, the ratio P_f is evaluated by counting the occurrence of $\Delta f^{(g)} > 0$. One has $L - 1$ differences for L values of $f_{\text{med}}^{(g)}$. Using the indicator function $\mathbb{1}$, the ratio yields

$$P_f = \frac{1}{L-1} \sum_{i=0}^{L-2} \mathbb{1}[\Delta f^{(g-i)} > 0]. \quad (24)$$

A threshold $\mathcal{T}_f = 1/5$ is chosen in [8] based on empirical studies and will be adopted. $P_f > \mathcal{T}_f$ triggers a population increase due to insufficient performance, for $P_f = \mathcal{T}_f$ no change occurs, and for $P_f < \mathcal{T}_f$ the population is decreased. As for all the PCS considered here, the respective threshold value \mathcal{T} has significant influence on the performance of the PCS and exchanging the CSA will lead to notable performance differences on simple test functions.

The pcCMSA was introduced in [6] and further analyzed in [16]. It was originally introduced as a covariance-matrix self-adaptive ES for population control on noisy functions and later tested on multimodal functions in [7]. In this paper, only the hypothesis test for convergence is implemented using a CSA, calling it pcCSA. In [6] it is argued that stagnation or divergence behavior coincides with a non-negative trend within the observed fitness value dynamics of the ES (for minimization). For a trend analysis, a regression model of the parental recombinant fitness sequence $f(\mathbf{y}^{(g)})$ of length L is used and a hypothesis test on the slope is done. The (fluctuating) fitness dynamics f is modeled assuming a linear model with slope a , intercept b , and random normal fluctuations ϵ_i as $f^{(g)} = ag + b + \epsilon_i$. Denoting the standard error of the estimated slope \hat{a} as $s_{\hat{a}}$, the (standardized) test statistic is a t -distributed variate with $L - 2$ degrees of freedom

$$T_{L-2} \sim (\hat{a} - a)/s_{\hat{a}}. \quad (25)$$

The hypothesis test is defined as $H_0: a \geq 0$, indicating no significant trend and insufficient performance. The alternative $H_1: a < 0$ indicates sufficient performance. We will evaluate the P -value of the test ($P_{t,L-2}$ denoting the distribution function of T with $L - 2$ degrees of freedom)

$$P_H := P_{t,L-2}(\hat{a}/s_{\hat{a}}), \quad (26)$$

rejecting H_0 at a significance level $P_H < 0.05$ ($\mathcal{T}_H = 0.05$). In this case, μ is decreased, or otherwise increased.

The core ideas of the PSA-CMA-ES were introduced in [17] and further extended in [7]. It is based on the idea of measuring the change of search space parameters, namely the covariance matrix \mathbf{C} and the mean search vector \mathbf{y} . By accumulating the information using two cumulation paths, their respective lengths are used as an indicator of ES performance. The key

Algorithm 2 Population Control Strategies (PCS)

 1: Measure performance \mathcal{P} in Alg. 1 by evaluation of:

get_apop()

 2: $\mathbf{d} \leftarrow \text{diff}(f_{\text{med}}^{(g_0:g)})$
 3: $P_f \leftarrow \text{sum}(\mathbf{d} > 0)/(L - 1)$
 4: $\mathcal{P} \leftarrow \text{perf}(P_f < \mathcal{T}_f: 1; P_f > \mathcal{T}_f: -1; P_f = \mathcal{T}_f: 0)$

get_pccsa()

 5: $\mathbf{g} \leftarrow [g_0 : g], \mathbf{f} \leftarrow [f_{\text{rec}}^{(g_0:g)}]$
 6: $\bar{g} \leftarrow \text{mean}(\mathbf{g}), \bar{f} \leftarrow \text{mean}(\mathbf{f})$
 7: $\hat{a} \leftarrow \frac{\sum_{i=1}^L (g_i - \bar{g})(f_i - \bar{f})}{\sum_{i=1}^L (g_i - \bar{g})^2}, \hat{b} \leftarrow \bar{f} - \hat{a}\bar{g}$
 8: $s_{\hat{a}} \leftarrow \sqrt{\frac{\sum_{i=1}^L (f_i - \bar{f})^2}{(L-2) \sum_{i=1}^L (g_i - \bar{g})^2}}$
 9: $t \leftarrow \hat{a}/s_{\hat{a}}$
 10: $P_H \leftarrow \text{tcdf}(t, L - 2) \quad \triangleright \text{distribution function of } T_{L-2}$
 11: $\mathcal{P} \leftarrow \text{perf}(P_H < \mathcal{T}_H: 1; P_H > \mathcal{T}_H: -1; P_H = \mathcal{T}_H: 0)$

get_psa()

 12: $E_F \leftarrow N/\mu^{(g)}$
 13: $\tilde{\Delta}_m \leftarrow \langle \mathbf{z} \rangle^{(g+1)}$
 14: $\tilde{\Delta}_c \leftarrow \frac{1}{\sqrt{2}}((\sigma^{(g+1)}/\sigma^{(g)})^2 - 1)\mathbf{1}$
 15: $\mathbf{p}_m^{(g+1)} \leftarrow (1 - \beta)\mathbf{p}_m^{(g)} + \sqrt{\beta(2 - \beta)}/E_F \tilde{\Delta}_m$
 16: $\mathbf{p}_c^{(g+1)} \leftarrow (1 - \beta)\mathbf{p}_c^{(g)} + \sqrt{\beta(2 - \beta)}/E_F \tilde{\Delta}_c$
 17: $\|\mathbf{p}_\theta^{(g+1)}\|^2 \leftarrow \|\mathbf{p}_m^{(g+1)}\|^2 + \|\mathbf{p}_c^{(g+1)}\|^2$
 18: $\mathcal{P} \leftarrow \text{perf}(\|\mathbf{p}_\theta\|^2 < \mathcal{T}_\theta: -1; \|\mathbf{p}_\theta\|^2 > \mathcal{T}_\theta: 1; \|\mathbf{p}_\theta\|^2 = \mathcal{T}_\theta: 0)$

element is to distinguish random selection (insufficient performance) from non-random selection (sufficient performance). The measured path lengths are used to change the population size, given a certain threshold. In contrast to pcCSA and APOP, the performance is measured solely in search space and not in f -space². The main idea is to define two cumulation paths for the change of the mean $\Delta \mathbf{m}^{(g+1)} = \mathbf{y}^{(g+1)} - \mathbf{y}^{(g)}$, and the change of \mathbf{C} and σ as $\Delta \Sigma^{(g+1)} = (\sigma^{(g+1)})^2 \mathbf{C}^{(g+1)} - (\sigma^{(g)})^2 \mathbf{C}^{(g)}$. Then, $\Delta \mathbf{m}^{(g+1)}$ and $\Delta \Sigma^{(g+1)}$ are transformed using their respective Fisher transformation matrices to achieve invariance w.r.t. the chosen (normal) search space distribution. Using a CSA-ES, i.e., $\mathbf{C} = \mathbf{I}$ (identity matrix), the update equations simplify significantly. The detailed derivation is presented in the supplementary material A-B. The corresponding cumulation paths from (A.11) and (A.13) yield

$$\mathbf{p}_m^{(g+1)} = (1 - \beta)\mathbf{p}_m^{(g)} + \sqrt{\beta(2 - \beta)\mu/N} \langle \mathbf{z} \rangle^{(g+1)}. \quad (27)$$

$$\mathbf{p}_c^{(g+1)} = (1 - \beta)\mathbf{p}_c^{(g)} + \sqrt{\frac{\beta(2 - \beta)\mu}{(2N)}} \left[\frac{(\sigma^{(g+1)})^2}{(\sigma^{(g)})^2} - 1 \right] \mathbf{1}, \quad (28)$$

with $\mathbf{1} = [1, \dots, 1]$ of length N . The PSA measures the squared norm of (27) and (28). Aggregating both vectors into a single update vector $\mathbf{p}_\theta^{(g+1)} = (\mathbf{p}_m^{(g+1)}, \mathbf{p}_c^{(g+1)})$, one evaluates

$$\|\mathbf{p}_\theta\|^2 = \|\mathbf{p}_m\|^2 + \|\mathbf{p}_c\|^2. \quad (29)$$

The results of (27) and (28) are notable. While (27) mirrors the cumulation of the CSA (using a different constant β and normalization w.r.t. N , see also CSA-update in (14)), cumulation (28) aggregates relative σ -changes. The PSA works

²Note that [7] and [17] elaborate the similarities between their update equations and the natural gradient interpretation of the CMA-ES. This is omitted at this point since we will investigate a simplification of the PSA-CMA-ES by only including the CSA without covariance matrix adaptation.

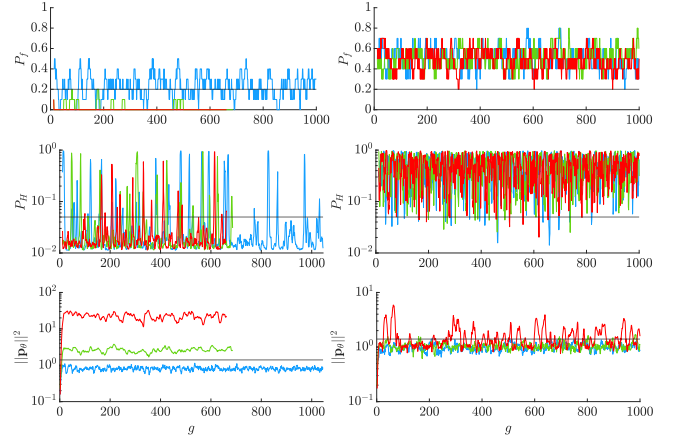


Fig. 5: Sphere (left column) and random function (right column) with CSA (17a) for $N = 100$ using APOP (top, $L = 10$), pcCSA (center, $L = 10$), and PSA (bottom $\beta = 1/10$). The performance is measured with deactivated population control at $\mu = 10, 100, 1000$ (blue, green, and red signals, respectively) The threshold \mathcal{T} is shown in solid black.

by measuring $\|\mathbf{p}_\theta\|^2 = \|\mathbf{p}_m\|^2 + \|\mathbf{p}_c\|^2$ and comparing it to the threshold $\mathcal{T}_\theta = 1.4$, cf. Fig. 8. Under random selection, one observes $\|\mathbf{p}_m\|^2 \approx 1$ and $\|\mathbf{p}_c\|^2 \approx 0$, which indicates insufficient performance ($\|\mathbf{p}_\theta\|^2 < \mathcal{T}_\theta$) and increases μ . Random selection with $\|\mathbf{p}_m\|^2 = 1$ can be obtained by evaluating $\|\mathbf{p}_m^{(g+1)}\|^2$ in (27). Assuming a steady-state in expectation, one has $\mathbb{E}[\|\mathbf{p}_m^{(g+1)}\|^2] = \mathbb{E}[\|\mathbf{p}_m^{(g)}\|^2] = \|\mathbf{p}_m\|^2$, $\mathbb{E}[\mathbf{p}_m^{(g)} \langle \mathbf{z} \rangle^{(g+1)}] = 0$ (no preferred search direction) and $\mathbb{E}[\|\langle \mathbf{z} \rangle\|^2] = N/\mu$ from [12, (5.2)], such that one simply gets $\|\mathbf{p}_m\|^2 = 1$. The analogous calculation holds for the steady-state $\mathbb{E}[\|\mathbf{s}\|^2] = N$ of the CSA under random selection. From the update rules (15) and (16) one infers that σ does not change in expectation. Hence, the contribution of (28) vanishes, giving $\|\mathbf{p}_c\|^2 = 0$. If the selection is not random, both $\|\mathbf{p}_m\|^2$ and $\|\mathbf{p}_c\|^2$ yield relevant contributions and the population is controlled to maintain $\|\mathbf{p}_\theta\|^2 \approx \mathcal{T}_\theta$. Analytic investigations of $\|\mathbf{p}_m\|^2$ and $\|\mathbf{p}_c\|^2$ in the sphere steady-state are given in the supplementary material A-C.

Before continuing the analysis, the performance measures of the PCS are evaluated with *deactivated* population control. In Fig. 5, the sphere (30a) and random function (30b) are evaluated at $N = 100$ for three constant μ -values. The respective quantities P_f , P_H , and $\|\mathbf{p}_\theta\|^2$ are measured. We are interested in the signal levels in relation to their thresholds. P_f from APOP decreases for increasing μ on f_{sph} . Larger populations yield less deterioration of the median fitness due to a more robust search. Note that at $\mu = 10$, $P_f > \mathcal{T}_f = 0.2$ most of the time. With active population control, this would trigger an (undesired) μ -increase on the sphere. On f_{ran} , the signals fluctuate around $P_f \approx 0.5$ (above \mathcal{T}_f), successfully indicating bad performance due to random selection. For the pcCSA, P_H mostly stays below the significance level $\mathcal{T}_H = 0.05$ on the sphere, which indicates good performance. On f_{ran} , P_H lies mostly above the threshold, correctly indicating bad performance. Sporadic f -fluctuations may (falsely) indicate

	L	β	α_μ	Δ_g	r_σ
P1	$\lceil N^{1/2} \rceil$	$1/N^{1/2}$	1.05	0	$(\mu^{(g+1)}/\mu^{(g)})^{1/2}$
P2	10	1/10	2	10	$(\mu^{(g+1)}/\mu^{(g)})^{1/2}$

TABLE I: Two parameter sets P1 and P2 for comparing the adaptive PCS.

good performance. For the PSA, $\|\mathbf{p}_\theta\|^2$ shows different levels depending on μ . At $\mu = 10$, $\|\mathbf{p}_\theta\|^2$ is smaller than the threshold $\mathcal{T}_\theta = 1.4$. At $\mu = 100, 1000$, it lies above it. Similar to the APOP, the PSA will increase μ on the sphere function to reach $\|\mathbf{p}_\theta\|^2 \approx 1.4$. This effect is due to the aggregation of relative σ -changes via (28) which increase for larger μ due to faster convergence (large $\|\mathbf{p}_c\|^2$ -contributions compared to $\|\mathbf{p}_m\|^2$, see supplementary material A-C). On the random function, the three signals lie in the vicinity of $\|\mathbf{p}_\theta\|^2 \approx 1$ mostly due to $\|\mathbf{p}_m\|^2 \approx 1$ and vanishing $\|\mathbf{p}_c\|^2 \approx 0$ (fluctuations can be observed). In general, the PSA detects random selection well.

A. Method Comparison

For the comparison of the introduced PCS, two sets of parameters will be chosen according to Tab. I by the following argumentation. The goal is to align the time scales of the PCS by which the performance of the ES is evaluated. Both pcCSA and APOP aggregate f -values over a length of L generations. Using the derived time scale (10), we set $L = \lceil N^{1/2} \rceil$ for P1. Similarly, the backward time horizon of the cumulation path scales as $1/\beta$, see [10]. To align the PSA with the array length L , we choose $\beta = 1/N^{1/2}$. Note that the CSA (17a) also operates at $c_\sigma = 1/N^{1/2}$. For P1 one chooses a small $\alpha_\mu = 1.05$, no waiting Δ_g , and r_σ (22b) according to Sec. IV to reduce the stress on the σ -adaptation ($\alpha_\mu = 1.05 \ll 2$). An alternative to P1 is the parameter set P2, including waiting times and performing larger μ -changes. This should stabilize the CSA additionally, see Fig. 4b. Since $G \propto \sqrt{N}$ scales weakly with N , one may choose a constant value $L = 10$ (and $\beta = 1/10$). As an example, $N = 10$ would yield $L = \lceil \sqrt{N} \rceil = 4$ and for $N = 1000$ one has $L = 32$. Both results are not too far away from $L = 10$. A constant L and β schedule was also applied in [8] and [7], however, large N were not investigated. Both sets require a comparable number of generations to reach $\mu_{\max} = 1024$ starting from $\mu_{\min} = 4$, with P1 yielding $g = 89$ and P2 $g = 78$ (if persistent μ -increase is triggered).

The test functions to be investigated are chosen as follows. The goal is to have a simple benchmark set to test basic, but essential properties of the PCS together with the underlying CSA. The properties are performance on a unimodal function, behavior under high noise, and performance on a highly multimodal function, all at varying dimensionality. To this end, we choose

$$f_{\text{sph}}(\mathbf{y}) := \sum_i^N y_i^2 \quad (30a)$$

$$f_{\text{ran}}(\mathbf{y}) := \mathcal{N}(0, 1) \quad (30b)$$

$$f_{\text{ras}}(\mathbf{y}) := \sum_i^N [y_i^2 + A(1 - \cos(\alpha y_i))]. \quad (30c)$$

On unimodal functions, the population size should be kept small to reduce the number of function evaluations. On the

	μ_{25}	μ_{med}	μ_{75}	F_t		μ_{25}	μ_{med}	μ_{75}	F_t
S10	14	20	37	1.1e+04	S10	8	16	32	1.2e+04
S100	23	95	318	3.3e+05	S100	16	16	32	4.5e+04
S1000	29	130	523	1.9e+06	S1000	16	16	32	2.0e+05
N10	1024	1024	1024	1.9e+06	N10	1024	1024	1024	1.9e+06
N100	1024	1024	1024	1.9e+06	N100	1024	1024	1024	1.9e+06
N1000	1024	1024	1024	1.8e+06	N1000	1024	1024	1024	1.9e+06
S10	129.5	1024	1024	2.7e+05	S10	4	4	8	3.7e+03
S100	4	4	7	1.8e+04	S100	4	4	8	1.8e+04
S1000	4	4	4	1.6e+05	S1000	4	4	8	1.7e+05
N10	1024	1024	1024	1.9e+06	N10	1024	1024	1024	1.8e+06
N100	1024	1024	1024	1.9e+06	N100	1024	1024	1024	1.8e+06
N1000	1024	1024	1024	1.8e+06	N1000	1024	1024	1024	1.7e+06
S10	13	17	20	6.6e+03	S10	8	8	16	5.0e+03
S100	33	41	56	6.7e+04	S100	32	32	64	6.9e+04
S1000	97	126	163	7.4e+05	S1000	256	256	512	1.4e+06
N10	29	37	56	8.6e+04	N10	16	32	64	1.1e+05
N100	343	594	927	1.2e+06	N100	256	512	1024	1.2e+06
N1000	1024	1024	1024	1.9e+06	N1000	1024	1024	1024	1.9e+06

TABLE II: CSA (17a) with APOP, pcCSA, PSA (top to bottom, respectively) with P1 and P2 (left and right column).

	μ_{25}	μ_{med}	μ_{75}	F_t		μ_{25}	μ_{med}	μ_{75}	F_t
S10	29	40	53	2.5e+04	S10	32	32	64	2.9e+04
S100	38	137	429	1.3e+06	S100	128	128	256	9.7e+05
S1000	37	177	761	1.5e+07	S1000	512	1024	1024	3.0e+07
N10	1024	1024	1024	1.9e+06	N10	1024	1024	1024	1.9e+06
N100	1024	1024	1024	1.9e+06	N100	1024	1024	1024	1.9e+06
N1000	1024	1024	1024	1.8e+06	N1000	1024	1024	1024	1.9e+06
S10	383	1024	1024	4.4e+05	S10	4	8	16	7.6e+03
S100	593	800	975	3.2e+06	S100	64	256	512	1.8e+06
S1000	11	18	31	9.4e+05	S1000	256	512	1024	2.3e+07
N10	1024	1024	1024	1.9e+06	N10	1024	1024	1024	1.8e+06
N100	1024	1024	1024	1.9e+06	N100	1024	1024	1024	1.8e+06
N1000	1024	1024	1024	1.8e+06	N1000	1024	1024	1024	1.7e+06
S10	29	33	37	1.9e+04	S10	8	16	16	1.0e+04
S100	429	474	550	2.1e+06	S100	256	512	512	2.4e+06
S1000	1024	1024	1024	4.1e+07	S1000	1024	1024	1024	4.1e+07
N10	133	201	287	4.3e+05	N10	64	128	256	4.0e+05
N100	1024	1024	1024	1.9e+06	N100	1024	1024	1024	1.9e+06
N1000	1024	1024	1024	1.9e+06	N1000	1024	1024	1024	1.9e+06

TABLE III: CSA (17b) with APOP, pcCSA, PSA (top to bottom, respectively) with P1 and P2 (left and right column).

	μ_{25}	μ_{med}	μ_{75}	F_t		μ_{25}	μ_{med}	μ_{75}	F_t
S10	438	689	975	2.3e+06	S10	1024	1024	1024	3.5e+06
S100	97	399	1024	1.6e+06	S100	128	512	1024	2.1e+06
S1000	32	147	594	2.0e+06	S1000	16	32	32	2.3e+05
N10	1024	1024	1024	1.9e+06	N10	1024	1024	1024	1.9e+06
N100	1024	1024	1024	1.9e+06	N100	1024	1024	1024	1.9e+06
N1000	1024	1024	1024	1.8e+06	N1000	1024	1024	1024	1.9e+06
S10	1024	1024	1024	4.3e+06	S10	512	1024	1024	3.1e+06
S100	4	6	9	2.0e+04	S100	4	4	8	1.9e+04
S1000	4	4	4	1.8e+05	S1000	4	4	8	1.8e+05
N10	1024	1024	1024	1.9e+06	N10	1024	1024	1024	1.8e+06
N100	1024	1024	1024	1.9e+06	N100	1024	1024	1024	1.8e+06
N1000	1024	1024	1024	1.8e+06	N1000	1024	1024	1024	1.7e+06
S10	928	1024	1024	4.1e+06	S10	16	16	32	2.4e+04
S100	40.5	59	103	2.8e+05	S100	32	64	512	6.2e+05
S1000	88	109	135	5.7e+05	S1000	128	256	256	1.3e+06
N10	740	974	1024	1.5e+06	N10	128	512	1024	1.1e+06
N100	761	1024	1024	1.7e+06	N100	512	1024	1024	1.4e+06
N1000	1023	1024	1024	1.8e+06	N1000	512	1024	1024	1.6e+06

TABLE IV: CSA (17c) with APOP, pcCSA, PSA (top to bottom, respectively) with P1 and P2 (left and right column).

random function, it should reach its maximum value and be kept large. The reason is that large populations reduce the expected residual distance for a sphere under high noise (see [1]). On the Rastrigin function, it should be dynamically changed since local attraction is only relevant within a certain range [2]. For both large and small $R^2 = \sum_i y_i^2$, f_{ras} behaves like a quadratic function.

A series of experiments on f_{sph} (denoted by ‘‘S’’) and f_{ran} (‘‘N’’ for noise) is shown in Tab. II, III, and IV. The number denotes the dimensionality (e.g. S10 is f_{sph} at $N = 10$). μ_{25} , μ_{med} , and μ_{75} measure the 25-th, 50-th, and 75-th percentile of the occurred $\mu^{(g)}$. They are an indicator of the overall μ -level and distribution width. F_t measures the number of function evaluations. Exemplary dynamics from the tables are shown in Figs. 6, 7, and 8. In general, one observes a high variation of

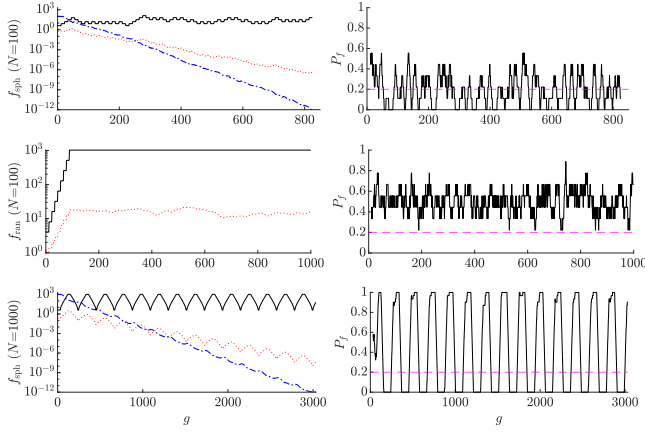


Fig. 6: APOP-dynamics with CSA (17a) for S100 (P2) at the top, N100 (P2) in the center, and undesired μ -oscillations for S1000 (P1) at the bottom.

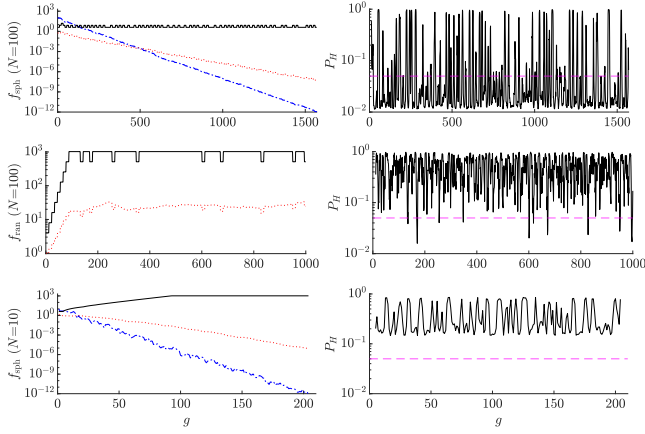


Fig. 7: pcCSA-dynamics with CSA (17a) for S100 (P2) at the top, N100 (P2) in the center, and undesired μ -increase for S10 (P1) at the bottom.

the performance on f_{sph} and f_{ran} , depending on the CSA. The best configuration for APOP and pcCSA is shown in Tab. II (CSA (17a)) for P2 (see top right and center right). They maintain low μ -levels on the f_{sph} and high, stable μ -levels on f_{ran} (examples in Figs. 6 and 7). The PSA shows mixed results (bottom right). The main issue is insufficient performance (low μ) for N10. This is critical, e.g., when optimizing multimodal functions at small N where high μ -levels are needed for global convergence. The overall best configuration for the PSA uses CSA (17c) (for which it was designed in [7]), see Tab. IV (P2, bottom right). However, it shows somewhat elevated μ -levels on f_{sph} (also reported by [7]).

Now the examples of Figs. 6, 7, and 8 are discussed in more detail. In the left plots, one has $\mu^{(g)}$ (solid black), $f^{(g)}$ (dash-dotted blue) and $\sigma^{(g)}$ (dotted red). On the right, the corresponding performance measures are shown in black with P_f (APOP), P_H (pcCSA), and $\|\mathbf{p}_\theta\|^2$ (PSA, $\|\mathbf{p}_m\|^2$ in blue and $\|\mathbf{p}_c\|^2$ in red). The threshold values are shown as dashed magenta. The respective top and center plots show examples where the PCS works relatively well. The bottom plot shows

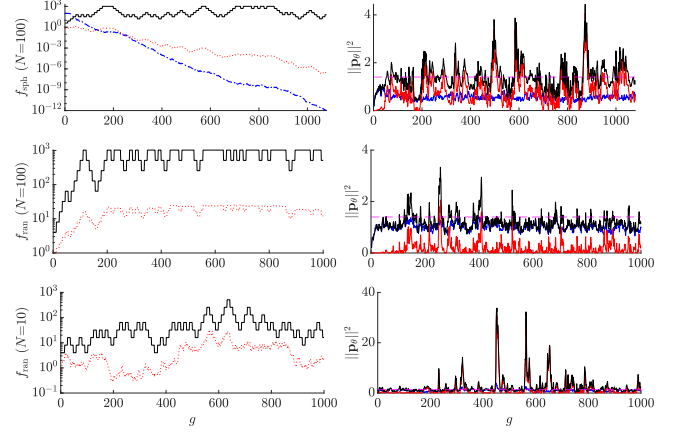


Fig. 8: PSA-dynamics with CSA (17c) for S100 (P2) at the top, N100 (P2) in the center, and insufficient μ -level for N10 with CSA (17a) at the bottom. On the right, one has $\|\mathbf{p}_\theta\|^2$ (black), $\|\mathbf{p}_m\|^2$ (blue), and $\|\mathbf{p}_c\|^2$ (red).

an example where undesired behavior was observed. Note that for f_{ran} no f -values are shown (random noise). The APOP in Fig. 6 on f_{sph} controls μ , such that P_f is close to the threshold 0.2. On f_{ran} , $P_f \approx 0.5$ lies above the threshold due to selection on a random function. Hence, μ is kept at the maximum value. In the bottom plot, zero waiting $\Delta_g = 0$ (via P1) introduces unnecessary oscillations of μ . They are related to constant changes of the f -distribution, such that (23) falsely detects fitness deterioration. Waiting $\Delta_g > 0$ is necessary to remove these issues (used in P2). An example of the changing f -distribution is shown in the supplementary material A-D. The pcCSA in Fig. 7 shows very low μ -levels on f_{sph} which is desired. On f_{ran} the hypothesis test detects stagnation reliably and keeps μ large. In the bottom plot, the small data set $L = \lceil N \rceil = 4$ yields large standard errors of (26), falsely indicating bad performance and increasing μ (example shown in the supplementary material A-E). The pcCSA requires a larger sample size L to overcome this issue (see P2 with $L = 10$). The PSA in Fig. 8 measures $\|\mathbf{p}_\theta\|^2$ (black) via $\|\mathbf{p}_m\|^2$ (blue) and $\|\mathbf{p}_c\|^2$ (red). On f_{sph} , $\|\mathbf{p}_m\|^2$ and $\|\mathbf{p}_c\|^2$ have similar contributions. On f_{ran} , $\|\mathbf{p}_m\|^2 \approx 1$ and $\|\mathbf{p}_c\|^2 \gtrsim 0$, indicating random selection (see discussion below (28)). However, fluctuations of σ may generate spurious larger $\|\mathbf{p}_c\|^2$ -contributions, yielding $\|\mathbf{p}_\theta\|^2$ above the threshold and reducing μ . The bottom example shows issues of the PSA to increase μ on f_{ran} due to the mentioned fluctuations. This occurs for CSA (17a), but is less pronounced for CSA (17c) since the latter adapts σ significantly slower due to $D \propto \sqrt{\mu/N}$ from (19). The PSA requires slow adaptation for small N to correctly detect random selection. Note that this effect is not related to the applied $r_\sigma = \sqrt{\mu^{(g+1)}/\mu^{(g)}}$, but to the underlying CSA (see supplementary material A-F).

One major observation can be made from Tab. III and IV. Recall that both CSAs (17b) and (17c) show increasingly slow adaptation within respective limits, see ratio approaching “1” in Fig. 2c. Very slow adaptation can significantly deteriorate the PCS performance on f_{sph} . In Tab. III, larger N show large

μ_{med} -levels and in Tab. IV, large μ_{med} -levels occur for small N . In general, bad performance at slow adaptation on f_{sph} can be explained in terms of measured f -values using Fig. 1b. Since the adaptation is very slow, the ES operates at very large σ^* close to $\sigma_{\varphi_0}^*$. It progresses very slowly and selects worse fitness values more often. The deterioration is reflected within the pcCSA by the hypothesis test mostly indicating stagnation. Similarly, the APOP counts significantly more worse fitness changes via (24), leading to unnecessary μ -increase on f_{sph} . The PSA shows mixed results. In Tab. III, it works well for S10 (small μ_{med}), but yields $\mu_{\text{med}} = \mu_{\text{max}}$ for S1000. It requires a different CSA, i.e., adaptation speed as a function of μ and N , to achieve better performance (see Tab. IV).

Comparing the experiments of parameter sets P1 and P2 in Tab. II, III, and IV shows mixed results. There are cases in which one option is either better or worse than the other and the results depend on both CSA and PCS. However, P2 with $\Delta_g > 0$ is preferred for APOP due to stability (see discussion of Fig. 6). Furthermore, P2 yields improved results for pcCSA (hypothesis test for small N) and in general good results for PSA. Hence, the parameter set P2 will be used as default in Sec. V-B for further investigations.

B. Comparison on the Rastrigin Function

Now that basic properties of the PCS- and CSA-variants have been studied on f_{sph} and f_{ran} , a simplified benchmark is performed on the Rastrigin function f_{ras} . The reason for choosing Rastrigin is that sufficiently large populations are needed to find the global attractor [2], [4]. However, local attraction has only a limited range, such that adaptive PCS should keep the population size small far away from the global attractor (global quadratic structure) and within a local (or global) attractor. The goal is to investigate the performance of the best configurations from Sec. V-A. Furthermore, the PCS will be compared against the CSA-variants with constant $\mu = \mu_{\text{max}}$.

The tested parameter sets of Rastrigin are chosen as follows. The first experiment is done at $N = 10, 30, 100, 300, 1000$ for constant multimodality parameters $A = 3$ and $\alpha = 2\pi$. Hence, f_{ras} becomes more difficult to optimize with increasing N . For the second experiment, one varies N and A together as $(N, A) = (10, 65), (30, 33), (100, 12), (300, 7), (1000, 3)$ (at $\alpha = 2\pi$). Large A are chosen for small N and vice-versa. The values are chosen such that CSA (17a) yields roughly a constant success rate $P_S \approx 0.9$ at $\mu = \mu_{\text{max}}$. The test provides “similar difficulty” for an ES operating at constant population size and will serve as a reference.

For the initialization, one chooses $\mathbf{y}^{(0)} = 2\lceil\alpha A/2\rceil \mathbf{1}$ (outside the local attraction region), $\sigma^{(0)} = \sigma_{\varphi_0}^* \|\mathbf{y}^{(0)}\|/N$ via (2) ensuring a large initial step-size, and $\mathbf{s}^{(0)} = \mathbf{1}$ for the CSA. The runs terminate for $f < f_{\text{stop}} = 10^{-3}$ (global convergence) or $\sigma < 10^{-3}$ with $f \geq f_{\text{stop}}$ (local convergence). For each parameter set, 50 trials are evaluated and the success rate P_S is measured. We measure the expected runtime E_r (in function evaluations) to reach global convergence by including

the number of function evaluations of successful (F_s) and unsuccessful (F_u) runs. For $P_S > 0$, it is estimated as [18]

$$E_r = (F_s + F_u)/P_S. \quad (31)$$

For the PCS, we choose the following parameters (see Sec. V-A)

$$\text{APOP: CSA (17a) and P2 (Tab. I)} \quad (32a)$$

$$\text{pcCSA: CSA (17a) and P2 (Tab. I)} \quad (32b)$$

$$\text{PSA: CSA (17c) and P2 (Tab. I).} \quad (32c)$$

The population size limits are $\mu^{(0)} = \mu_{\text{min}} = 4$ and $\mu_{\text{max}} = 1024$. There are two reasons for limiting μ . One reason are limited computational resources, especially when optimizing Rastrigin at large $N = 1000$. The second reason is that the PCS are compared to constant $\mu = \mu_{\text{max}}$ runs. Certain examples will show that μ_{max} is not reached by the PCS, even though it should be reached to achieve better performance.

The results are shown in Fig. 9 in terms of P_S and E_r . The following observations can be made. At constant $\mu = \mu_{\text{max}}$, CSA (17a) yields a very good overall performance. While P_S is comparable to CSA (17b) and (17c), its E_r levels are the lowest (only exception is $N = 10$ in Fig. 9b). While E_r remains approximately constant in Fig. 9b, CSA (17b) and (17c) show notable upward and downward trends for E_r , respectively, due to their different adaptation characteristics. With active μ -control, APOP and pcCSA stay mostly below $\mu = \mu_{\text{max}}$ of CSA (17a) (the CSA they utilize). This is important as it illustrates a more effective search with active μ -control. The highest efficiency (lowest E_r) for small N are achieved by pcCSA, which is related to very low μ -levels in the sphere limits (see Tab. II). However, the pcCSA shows a significant drop in P_S (and increase of E_r) for large N . The APOP shows very good overall results, showing relatively high P_S -levels and satisfactory E_r for the tested configurations. However, its performance also decreases to some extent for large N . The PSA shows lower E_r -values than its CSA (17c) at $\mu = \mu_{\text{max}}$, which is good. In Fig. 9b, its E_r -slope closely follows CSA (17c) which illustrates that the CSA properties are recovered with active population control. In contrast to APOP and pcCSA, the PSA performs best at large $N = 1000$. At small $N = 10$, it tends to pick up more fluctuations of σ that falsely indicate good performance when measuring $\|\mathbf{p}_\theta\|^2$ (similar to the bottom plot in Fig. 8). At large N , the fluctuations of the contributing terms $\|\mathbf{p}_m\|^2$ and $\|\mathbf{p}_c\|^2$ are reduced and the detection of insufficient performance becomes more robust. Exemplary dynamics of the PCS on f_{ras} are given in the supplementary material A-G.

Figure 10 shows the same experiment as in Fig. 9, now with σ -rescaling r_σ being varied for each of the three PCS. For APOP one observes improved P_S (left) and E_r (right) for (22b) most of the time. For pcCSA mixed results are obtained. Either (22b) or (22c) yields higher P_S and lower E_r , respectively. Similar (mixed) results are observed for PSA. Linear scaling improves E_r for small N in Fig. 10b, but not at large N . Recall that linear scaling was originally used by [7] (see also discussion of (13)). In nearly all cases, no rescaling (22a) yields worse results for all PCS. The stability tests with

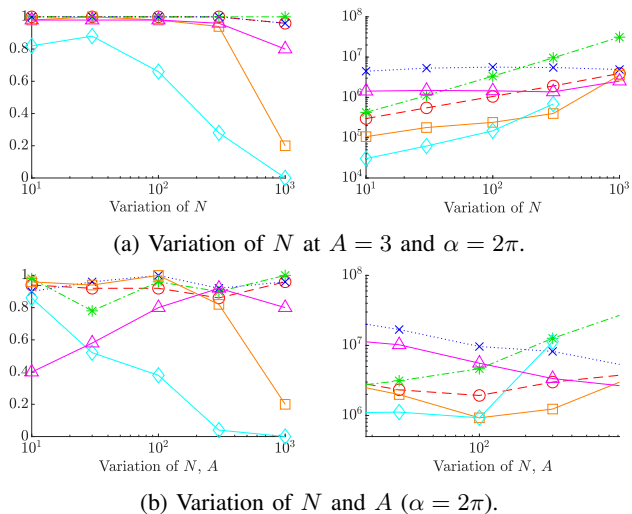


Fig. 9: Success rate P_S (left column) and expected runtime E_r (right column) on f_{ras} . The CSA with $\mu = \mu_{\text{max}}$ are shown as \circ (17a), $*$ (17b), and \times (17c). The PCS are shown as \square (32a), \diamond (32b), and \triangle (32c).

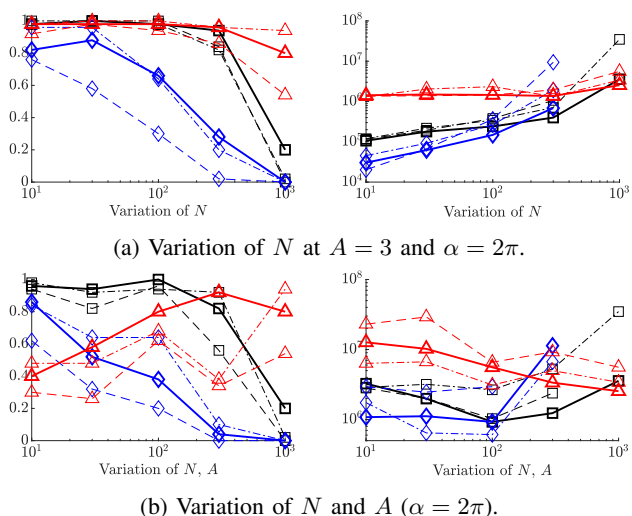


Fig. 10: Setup as shown in Fig. 9. The PCS are shown as \square (32a), \diamond (32b), and \triangle (32c). Given P2 in Tab. I, rescaling r_σ is varied using (22b) (solid, bold, same data as in Fig. 9), (22c) (dash-dotted), and (22a) (dashed).

predefined μ -schedule in Sec. IV have shown clear advantages of (22b), which is not observed in Fig. 10. Using active PCS introduces feedback that controls μ based on the measured \mathcal{P} . The realized changes in μ (over multiple generations) are usually moderate compared to a fixed schedule. This leads to smaller σ -changes due to rescaling. Furthermore, the waiting time $\Delta_g > 0$ helps to stabilize the σ -dynamics for any r_σ , see also Fig. 4b. Experiments on f_{sph} and f_{ran} with varying r_σ (not shown) yield similar inconclusive results. The only exception is the PSA which (on the sphere) appears more susceptible to larger changes of (22c) due to its aggregation (28).

VI. CONCLUSIONS AND OUTLOOK

In this paper, adaptive (online) population control strategies (PCS) were investigated for a multi-recombinative $(\mu/\mu_I, \lambda)$ -ES with cumulative step-size adaptation (CSA) and isotropic mutations. To this end, the adaptation properties of standard CSA-variants were discussed on the sphere as a function of population size μ and dimensionality N . Furthermore, scaling laws for the generation number (\sqrt{N} -law, independent of μ) and rescaling of the mutation strength ($\sqrt{\mu}$ -law) were derived on the sphere in the limit of large population sizes.

The obtained scaling laws were implemented into three state-of-the-art PCS, namely APOP [8], pcCSA [6], and PSA [7]. The experimental (and theoretical) analysis of the PCS has shown significant dependence of their respective performance measures on the CSA-variants. On the selected test bed (sphere, random, and Rastrigin functions), APOP and pcCSA using CSA (17a) (cumulation constant = $1/\sqrt{N}$, damping = \sqrt{N}) perform well due to comparably fast σ -adaptation. This improves overall progress and also helps the PCS to discern good from insufficient ES-performance. PSA works more efficiently using CSA (17c) due to its underlying cumulation paths. Especially on the Rastrigin function, the PCS benefit from short data aggregation periods (\sqrt{N} -law) together with equally short waiting times for the decorrelation of μ -dependent data. For σ -rescaling r_σ , stability tests on the sphere have shown clear advantages of a $\sqrt{\mu}$ -law. However, with active PCS the effects of r_σ are less pronounced. Strengths and weaknesses of the individual PCS have been discussed. In conclusion, there is no clear winner among the PCS. Best overall performance was achieved by APOP, providing good results across all parameter variations. On the other hand, pcCSA was the most efficient PCS at low N , while PSA achieved the best results at large N .

Of course, the performance of individual PCS can be improved by selective parameter tuning. However, as the aim of the present work was to investigate basic properties of CSA and PCS, this is left for future research. Further research aims at testing favorable PCS configurations on a larger benchmark set of noisy and multimodal functions. The goal is to have good performance over a large dimensionality range, while maintaining efficiency on unimodal functions. Another potential line of research is the improvement (or hybridization) of different population control methods, which may evaluate the ES performance in both search and fitness space. Future research should also investigate the interaction of PCS with active covariance matrix adaptation (CMA). These investigations should, hopefully, yield improved algorithms that perform well on a variety of test functions and also scale well with the dimensionality.

REFERENCES

- [1] D. Arnold and H.-G. Beyer, "Performance Analysis of Evolution Strategies with Multi-Recombination in High-Dimensional \mathbb{R}^N -Search Spaces Disturbed by Noise," *Theoretical Computer Science*, vol. 289, pp. 629–647, 2002.
- [2] L. Schönerberger and H.-G. Beyer, "On a Population Sizing Model for Evolution Strategies Optimizing the Highly Multimodal Rastrigin Function," in *Proceedings of the Genetic and Evolutionary Computation Conference*, ser. GECCO '23, New York, NY, USA, 2023, p. 848–855. [Online]. Available: <https://doi.org/10.1145/3583131.3590451>

- [3] A. Omeradzic and H.-G. Beyer, “Convergence Properties of the $(\mu/\mu_I, \lambda)$ -ES on the Rastrigin Function,” in *Proceedings of the 17th ACM/SIGEVO Conference on Foundations of Genetic Algorithms*, ser. FOGA '23. New York, NY, USA: Association for Computing Machinery, 2023, p. 117–128. [Online]. Available: <https://doi.org/10.1145/3594805.3607126>
- [4] —, “Self-Adaptation of Multi-Recombinant Evolution Strategies on the Highly Multimodal Rastrigin Function,” *IEEE Transactions on Evolutionary Computation*, 2024. [Online]. Available: <https://doi.org/10.1109/TEVC.2024.3400857>
- [5] H.-G. Beyer and B. Sendhoff, “Evolution Strategies for Robust Optimization,” in *Proceedings of the WCCI'06 Conference*. Piscataway, NJ: IEEE Press, 2006, pp. 4489–4496.
- [6] M. Hellwig and H.-G. Beyer, “Evolution under Strong Noise: A Self-Adaptive Evolution Strategy Can Reach the Lower Performance Bound - the pcCMSA-ES,” in *Parallel Problem Solving from Nature XXIV*, E. Hart et al., Ed. Berlin: Springer, 2016, pp. 26–36, https://doi.org/10.1007/978-3-319-45823-6_3.
- [7] K. Nishida and Y. Akimoto, “PSA-CMA-ES: CMA-ES with Population Size Adaptation,” in *Proceedings of the Genetic and Evolutionary Computation Conference*, ser. GECCO '18. New York, NY, USA: Association for Computing Machinery, 2018, p. 865–872. [Online]. Available: <https://doi.org/10.1145/3205455.3205467>
- [8] D. M. Nguyen and N. Hansen, “Benchmarking CMAES-APOP on the BBOB Noiseless Testbed,” in *Proceedings of the Genetic and Evolutionary Computation Conference Companion*, ser. GECCO '17. New York, NY, USA: Association for Computing Machinery, 2017, p. 1756–1763. [Online]. Available: <https://doi.org/10.1145/3067695.3084207>
- [9] N. Hansen, A. Auger, R. Ros, O. Mersmann, T. Tušar, and D. Brockhoff, “COCO: A platform for comparing continuous optimizers in a black-box setting,” *Optimization Methods and Software*, vol. 36, pp. 114–144, 2021.
- [10] N. Hansen, “The CMA Evolution Strategy: A Tutorial,” 2023. [Online]. Available: <https://www.arxiv.org/abs/1604.00772>
- [11] N. Hansen and A. Ostermeier, “Completely Derandomized Self-Adaptation in Evolution Strategies,” *Evolutionary Computation*, vol. 9, no. 2, pp. 159–195, 2001, <https://doi.org/10.1162/106365601750190398>.
- [12] D. Arnold, *Noisy Optimization with Evolution Strategies*. Dordrecht: Kluwer Academic Publishers, 2002.
- [13] H.-G. Beyer, *The Theory of Evolution Strategies*, ser. Natural Computing Series. Heidelberg: Springer, 2001, DOI: 10.1007/978-3-662-04378-3.
- [14] A. Omeradzic and H.-G. Beyer, “Mutation Strength Adaptation of the $(\mu/\mu_I, \lambda)$ -ES for Large Population Sizes on the Sphere Function,” 2024. [Online]. Available: <https://arxiv.org/abs/2408.09761>
- [15] N. Hansen, “Verallgemeinerte individuelle Schrittweitenregelung in der Evolutionsstrategie,” Doctoral thesis, Technical University of Berlin, Berlin, 1998.
- [16] H.-G. Beyer and M. Hellwig, “Analysis of the pcCMSA-ES on the noisy ellipsoid model,” in *GECCO'17: Proceedings of the Genetic and Evolutionary Computation Conference*. New York: ACM, 2017, pp. 689–696, DOI: 10.1145/3071178.3079195.
- [17] K. Nishida and Y. Akimoto, “Population size adaptation for the CMA-ES based on the estimation accuracy of the natural gradient,” in *GECCO'16: Proceedings of the Genetic and Evolutionary Computation Conference*. New York: ACM, 2016, pp. 237–244.
- [18] A. Auger and N. Hansen, “Performance Evaluation of an Advanced Local Search Evolutionary Algorithm,” in *Congress on Evolutionary Computation, CEC'05*, vol. 2. IEEE, 2005, pp. 1777–1784.
- [19] M. Nomura, Y. Akimoto, and I. Ono, “CMA-ES with Learning Rate Adaptation: Can CMA-ES with Default Population Size Solve Multimodal and Noisy Problems?” in *Proceedings of the Genetic and Evolutionary Computation Conference*, ser. GECCO '23, New York, NY, USA, 2023, p. 839–847. [Online]. Available: <https://doi.org/10.1145/3583131.3590358>

APPENDIX A
SUPPLEMENTARY MATERIAL

A. Mutation Strength Rescaling

In this section, the rescaling of the mutation strength σ of the PSA from [7] is analyzed. It will be shown that for sufficiently large N it corresponds to result (13), i.e., a linear relation between mutation strengths and population sizes. The σ -change introduced in [7, (17)] agrees with the form $\sigma^{(g+1)} = r_\sigma \sigma^{(g)}$ of III-A. The authors use an optimal σ^* derived from a quality gain analysis on the sphere as

$$\sigma^* = \frac{c\mu_w N}{N-1+c^2\mu_w}. \quad (\text{A.1})$$

A few remarks on (A.1) are given. Note that $\mu_w = \mu$ for intermediate recombination. Furthermore, the coefficient c is given as the sum $c = -\sum_{i=1}^\lambda w_i \mathbb{E}[\mathcal{N}_{i;\lambda}] = -\frac{1}{\mu} \sum_{i=1}^\mu \mathbb{E}[\mathcal{N}_{i;\lambda}]$ for $w_i = 1/\mu$ ($1 \leq i \leq \mu$) and $w_i = 0$ ($\mu < i \leq \lambda$). The coefficient c can be related to the progress coefficient $c_{\mu/\mu,\lambda}$ using [12, (D.33)]. Assuming zero noise and the case of minimization, one has ($h_{\mu,\lambda}^{1,0} = c_{\mu/\mu,\lambda}$), such that

$$c = -\frac{1}{\mu} \sum_{i=1}^\mu \mathbb{E}[\mathcal{N}_{i;\lambda}] = -\frac{1}{\mu} \sum_{i=1}^\mu \mathbb{E}[z_{i;\lambda}] = c_{\mu/\mu,\lambda}. \quad (\text{A.2})$$

Hence, (A.1) yields for intermediate recombination

$$\sigma^* = \frac{c_{\mu/\mu,\lambda}\mu N}{N-1+c_{\mu/\mu,\lambda}^2\mu} \stackrel{N \rightarrow \infty}{\simeq} c_{\mu/\mu,\lambda}\mu. \quad (\text{A.3})$$

The result (A.3) yields the optimal $\hat{\sigma}^* = c_{\mu/\mu,\lambda}\mu$ for $N \rightarrow \infty$ and $\mu \ll N$, which agrees with the σ^* maximizing (12). These results correspond to a rescaling of σ linear with the population size, as shown in (13). However, the limit $\mu \rightarrow \infty$ ($N < \infty$) yields the asymptotic $\frac{c_{\mu/\mu,\lambda}\mu N}{N-1+c_{\mu/\mu,\lambda}^2\mu} \simeq \frac{N}{c_{\mu/\mu,\lambda}}$, which does not recover the square root law derived in (11).

B. PSA-CSA-ES Analysis

In this section, the analysis of the simplified PSA-CMA-ES from [7] is shown. To this end, only the CSA-ES is considered without covariance matrix adaptation. Furthermore, intermediate recombination is used. These assumptions, along with the normalization in (A.8), will allow to derive the corresponding cumulation paths (27) and (28) of the PSA.

The main idea of the PSA is to define two cumulation paths for the change of the mean search vector $\mathbf{y}^{(g)}$ and the covariance matrix $\mathbf{C}^{(g)}$. One measures $\Delta \mathbf{m}^{(g+1)} = \mathbf{y}^{(g+1)} - \mathbf{y}^{(g)}$ for the positional change. For the change of the covariance matrix \mathbf{C} and the mutation strength σ , one defines $\Sigma^{(g)} = (\sigma^{(g)})^2 \mathbf{C}^{(g)}$ first. Then, one evaluates the difference $\Delta \Sigma^{(g+1)} = (\sigma^{(g+1)})^2 \mathbf{C}^{(g+1)} - (\sigma^{(g)})^2 \mathbf{C}^{(g)}$. Furthermore, $\Delta \mathbf{m}^{(g+1)}$ and $\Delta \Sigma^{(g+1)}$ are transformed using their respective Fisher transformation matrices (details in [19]) to achieve invariance w.r.t. the chosen (normal) search space distribution. The transformed quantities are [19, (15a),(15b)]

$$\tilde{\Delta \mathbf{m}}^{(g+1)} = \sqrt{\Sigma^{(g)}}^{-1} \Delta \mathbf{m}^{(g+1)} \quad (\text{A.4})$$

$$\tilde{\Delta \Sigma}^{(g+1)} = \frac{1}{\sqrt{2}} \text{vec} \left(\sqrt{\Sigma^{(g)}}^{-1} \Delta \Sigma^{(g+1)} \sqrt{\Sigma^{(g)}}^{-1} \right). \quad (\text{A.5})$$

The inverse matrix square root is denoted by $\sqrt{\Sigma}^{-1}$ (see also [10] for more details on the transformation). Furthermore, $\text{vec}(\cdot)$ denotes the transformation of the argument (matrix) into a vector form for the cumulation path. Using cumulation constant β , the PSA measures the two update paths (cf. [7, (12)])

$$\mathbf{p}_m^{(g+1)} = (1-\beta)\mathbf{p}_m^{(g)} + \sqrt{\beta(2-\beta)/E_F} \tilde{\Delta \mathbf{m}}^{(g+1)} \quad (\text{A.6})$$

$$\mathbf{p}_c^{(g+1)} = (1-\beta)\mathbf{p}_c^{(g)} + \sqrt{\beta(2-\beta)/E_F} \tilde{\Delta \Sigma}^{(g+1)}. \quad (\text{A.7})$$

The quantity E_F includes the expected value of the Fisher-transformed updates $\tilde{\Delta \mathbf{m}}$ and $\tilde{\Delta \Sigma}$, see [7, (13)] and serves as a normalization factor. For inactive matrix adaptation, only the first two terms are relevant giving $E_F \approx \frac{N}{\mu} + \frac{2N(N-E_\chi^2)}{E_\chi^2} \gamma_\sigma^{(g+1)} \frac{c_\sigma^2}{d_\sigma^2}$ (where $\gamma_\sigma^{(g+1)} \rightarrow 1$ is a time-dependent quantity quickly approaching one and $E_\chi^2 \propto N$). For sufficiently small ratios $c_\sigma^2/d_\sigma^2 \ll 1$ (which is usually satisfied for $c_\sigma^{-1} \propto d_\sigma$), the second term is negligible and we can approximate

$$E_F \approx N/\mu. \quad (\text{A.8})$$

The PSA measures the squared norm of both contributions (A.6) and (A.7). Aggregating both vectors into a single update vector $\mathbf{p}_\theta^{(g+1)} = (\mathbf{p}_m^{(g+1)}, \mathbf{p}_c^{(g+1)})$, one evaluates

$$\|\mathbf{p}_\theta\|^2 = \|\mathbf{p}_m\|^2 + \|\mathbf{p}_c\|^2. \quad (\text{A.9})$$

The result (A.9) is discussed below (29).

Now the simplified evolution paths are evaluated. Note that without covariance matrix adaptation, one has $\Sigma = \sigma^2 \mathbf{I}$ with inverse square root $\sqrt{\Sigma}^{-1} = \frac{1}{\sigma} \mathbf{I}$. The position update yields $\mathbf{y}^{(g+1)} = \mathbf{y}^{(g)} + \frac{1}{\mu} \sum_{m=1}^\mu \mathbf{x}_{m;\lambda}$ with $\mathbf{x}_{m;\lambda}$ denoting the selection of the $m = 1, \dots, \mu$ best mutations, see Alg. 1. Hence, one obtains for (A.4) with $\mathbf{x} = \sigma \mathbf{z}$ and $\mathbf{z} \sim \mathcal{N}(\mathbf{0}, \mathbf{1})$

$$\begin{aligned} \tilde{\Delta \mathbf{m}}^{(g+1)} &= \frac{1}{\sigma^{(g)}} \mathbf{I} \left(\mathbf{y}^{(g+1)} - \mathbf{y}^{(g)} \right) \\ &= \frac{1}{\mu} \sum_{m=1}^\mu \mathbf{z}_{m;\lambda} = \langle \mathbf{z} \rangle^{(g+1)}. \end{aligned} \quad (\text{A.10})$$

By inserting (A.10) and (A.8) into (A.6), one gets the same form as the CSA cumulation path (14) with additional normalization factor $1/\sqrt{N}$

$$\mathbf{p}_m^{(g+1)} = (1-\beta)\mathbf{p}_m^{(g)} + \sqrt{\beta(2-\beta)\mu/N} \langle \mathbf{z} \rangle^{(g+1)}. \quad (\text{A.11})$$

Now (A.5) is evaluated using $\sqrt{\Sigma}^{-1} = \frac{1}{\sigma} \mathbf{I}$. One gets

$$\begin{aligned} \tilde{\Delta \Sigma} &= \frac{1}{\sqrt{2}} \text{vec} \left(\frac{1}{\sigma^{(g)}} \mathbf{I} \left[(\sigma^{(g+1)})^2 \mathbf{I} - (\sigma^{(g)})^2 \mathbf{I} \right] \frac{1}{\sigma^{(g)}} \mathbf{I} \right) \\ &= \frac{1}{\sqrt{2}} \text{vec} \left(\left[\frac{(\sigma^{(g+1)})^2}{(\sigma^{(g)})^2} - 1 \right] \mathbf{I} \right) = \frac{1}{\sqrt{2}} \left[\frac{(\sigma^{(g+1)})^2}{(\sigma^{(g)})^2} - 1 \right] \mathbf{1}. \end{aligned} \quad (\text{A.12})$$

The notation $\mathbf{1} = [1, \dots, 1]$ (with length N) was used. For the vectorization of the identity, one may use $\text{vec}(\mathbf{I}) = \mathbf{1}$ by considering only the non-zero elements since the aggregation of constant zero values is useless. Hence, the update rule yields

$$\mathbf{p}_c^{(g+1)} = (1-\beta)\mathbf{p}_c^{(g)} + \sqrt{\frac{\beta(2-\beta)\mu}{(2N)}} \left[\frac{(\sigma^{(g+1)})^2}{(\sigma^{(g)})^2} - 1 \right] \mathbf{1}. \quad (\text{A.13})$$

C. Sphere Steady-State of the PSA-CSA-ES

In this section, sphere steady-state contributions of $\|\mathbf{p}_m\|^2$ and $\|\mathbf{p}_c\|^2$ (see (29) or (A.9)) are derived by assuming a constant population size μ . As already mentioned, the cumulation path of $\|\mathbf{p}_m\|^2$ works analogously to the cumulation of the CSA-ES (cf. (27) and (14)). Hence, one may directly apply the steady-state derivation of the CSA from [14] to the derivation of $\|\mathbf{p}_m\|^2$. Only the main derivation steps are recalled now. The derivation requires the evaluation of $\|\mathbf{p}_m^{(g+1)}\|^2$. Assuming that progress on the sphere is achieved along a certain component A (unit vector $\mathbf{e}_A^{(g)}$) with the remaining $N-1$ components being selectively neutral, a second equation of $\mathbf{p}_m^{(g+1)}$ along direction A is derived, such that one has to evaluate the scalar product

$$p_A^{(g+1)} = \mathbf{p}_m^{(g+1)} \mathbf{e}_A^{(g+1)}. \quad (\text{A.14})$$

In order to obtain closed-form solutions of the steady-state, approximations are applied in [14] by assuming sufficiently small progress rates. Then, one imposes the steady-state conditions (in expectation) by setting $\mathbb{E} \left[\left\| \mathbf{p}_m^{(g+1)} \right\|^2 \right] = \left\| \mathbf{p}_m^{(g)} \right\|^2 = \|\mathbf{p}_m\|^2$ and $\mathbb{E} \left[p_A^{(g+1)} \right] = p_A^{(g)} = p_A$. One obtains expected values over the selected mutation direction, i.e., $\mathbb{E} [\|\langle \mathbf{z} \rangle\|^2]$ and $\mathbb{E} [\langle z_A \rangle]$ with $\langle z_A \rangle = \langle \mathbf{z} \rangle \mathbf{e}_A$. Accounting for the fact that the cumulation constant of PSA is β (instead of c_σ) and the normalization of the cumulation path includes $\sqrt{\mu/N}$ (instead of only $\sqrt{\mu}$), one obtains the steady-state equation for p_A (analogous equation to [14, (30)]) as

$$p_A = \sqrt{\frac{\beta(2-\beta)\mu \mathbb{E} [\langle z_A \rangle] - \frac{\sigma^*}{N} \mathbb{E} [\|\langle \mathbf{z} \rangle\|^2]}{N \beta + (1-\beta) \frac{\sigma^*}{N} \mathbb{E} [\langle z_A \rangle]}}. \quad (\text{A.15})$$

Similarly, one gets for the squared norm the steady-state equation (cf. [14, (31)])

$$\|\mathbf{p}_m\|^2 = \frac{\mu}{N} \mathbb{E} [\|\langle \mathbf{z} \rangle\|^2] + \frac{2(1-\beta)}{\beta(2-\beta)} \sqrt{\frac{\beta(2-\beta)\mu}{N}} p_A \mathbb{E} [\langle z_A \rangle] \quad (\text{A.16})$$

Now (A.15) can be inserted into (A.16), which yields

$$\begin{aligned} \|\mathbf{p}_m\|^2 &= \frac{\mu}{N} \mathbb{E} [\|\langle \mathbf{z} \rangle\|^2] \\ &+ \frac{2(1-\beta)\mu \mathbb{E} [\langle z_A \rangle]^2 - \frac{\sigma^*}{N} \mathbb{E} [\langle z_A \rangle] \mathbb{E} [\|\langle \mathbf{z} \rangle\|^2]}{N \beta + (1-\beta) \frac{\sigma^*}{N} \mathbb{E} [\langle z_A \rangle]}. \end{aligned} \quad (\text{A.17})$$

The expected values in (A.17) are known quantities. One has

$$\mathbb{E} [\langle z_A \rangle] = \sqrt{2N} c_\sigma / \sigma^*, \quad \text{from [12, (5.7)],} \quad (\text{A.18a})$$

$$\text{with } \sqrt{1 + \sigma^{*2}/2N} \simeq \sigma^* / \sqrt{2N}, \quad c_{\mu/\mu, \lambda} \simeq c_\sigma$$

$$\mathbb{E} [\|\langle \mathbf{z} \rangle\|^2] = N/\mu, \quad \text{from [12, (5.2)].} \quad (\text{A.18b})$$

Hence, (A.17) can be evaluated as

$$\|\mathbf{p}_m\|^2 = 1 + 2(1-\beta) \frac{\frac{2c_\sigma^2 \mu}{\sigma^{*2}} - \sqrt{2/N} c_\sigma}{\beta + (1-\beta) \sqrt{2/N} c_\sigma}. \quad (\text{A.19})$$

Result (A.19) is a function of the normalized mutation strength σ^* . Therefore, the steady-state $\|\mathbf{p}_m\|^2$ depends on the CSA-parametrization. It is now useful to apply assumption (8) to

express the steady-state $\sigma^* = \sigma_{\text{ss}}^*(\gamma)$ as a function of scaling parameter γ , such that one gets

$$\begin{aligned} \|\mathbf{p}_m\|^2 &= 1 + 2(1-\beta) \frac{\frac{2c_\sigma^2 \mu}{\gamma^2 (8N)^{1/2} c_\sigma \mu} - \sqrt{2/N} c_\sigma}{\beta + (1-\beta) \sqrt{2/N} c_\sigma} \\ &= 1 + 2(1-\beta) \frac{\sqrt{2/N} c_\sigma \left(\frac{1}{2\gamma^2} - 1 \right)}{\beta + (1-\beta) \sqrt{2/N} c_\sigma}, \end{aligned} \quad (\text{A.20})$$

such that after rearranging one finally gets

$$\|\mathbf{p}_m\|^2 = 1 - \frac{2 - 1/\gamma^2}{1 + \frac{\beta}{\sqrt{2/N} c_\sigma (1-\beta)}}. \quad (\text{A.21})$$

For sufficiently slow adaptation, i.e., in the limit $\gamma \rightarrow 1$, (A.21) is expected to yield $\|\mathbf{p}_m\|^2 < 1$ (see also Fig. 11).

Now the steady-state of $\|\mathbf{p}_c\|^2$ is derived. For brevity the following notation is introduced for the relative σ -change derived in (A.13)

$$s := \left(\sigma^{(g+1)} / \sigma^{(g)} \right)^2 - 1. \quad (\text{A.22})$$

The cumulation path yields ($\mathbf{1} = [1, \dots, 1]$, $\sum_i \mathbf{1} = N$)

$$\mathbf{p}_c^{(g+1)} = (1-\beta) \mathbf{p}_c^{(g)} + \sqrt{\frac{\beta(2-\beta)\mu}{2N}} s \mathbf{1}. \quad (\text{A.23})$$

Assuming the steady-state $\mathbf{p}_c = \mathbf{p}_c^{(g)} = \mathbf{p}_c^{(g+1)}$, (A.23) yields

$$\mathbf{p}_c = \frac{1}{\beta} \sqrt{\frac{\beta(2-\beta)\mu}{2N}} s \mathbf{1}. \quad (\text{A.24})$$

By squaring the result (A.24), one gets

$$\|\mathbf{p}_c\|^2 = \left(\frac{1}{\beta} - \frac{1}{2} \right) \mu s^2. \quad (\text{A.25})$$

Assuming the steady-state in expectation, the expected value of the result in (A.25) yields

$$\mathbb{E} [\|\mathbf{p}_c\|^2] = \|\mathbf{p}_c\|^2 = \left(\frac{1}{\beta} - \frac{1}{2} \right) \mu \mathbb{E} [s^2]. \quad (\text{A.26})$$

As the next step, the relative σ -change s will be expressed as a function of the progress rate on the sphere. From (2) it holds $\sigma^{(g+1)} / \sigma^{(g)} = R^{(g+1)} / R^{(g)}$ for a constant $\sigma^{*,(g+1)} = \sigma^{*,(g)}$ in the sphere steady-state. One can rewrite $\mathbb{E} [s^2]$ as

$$\begin{aligned} \mathbb{E} [s^2] &= \mathbb{E} \left[\left(\left(\frac{\sigma^{(g+1)}}{\sigma^{(g)}} \right)^2 - 1 \right)^2 \right] = \mathbb{E} \left[\left(\left(\frac{R^{(g+1)}}{R^{(g)}} \right)^2 - 1 \right)^2 \right] \\ &= \mathbb{E} \left[\left(\frac{R^{(g+1)}}{R^{(g)}} \right)^4 - 2 \left(\frac{R^{(g+1)}}{R^{(g)}} \right)^2 + 1 \right]. \end{aligned} \quad (\text{A.27})$$

One can now look at the sphere quality gain to obtain an expression for the relation $\mathbb{E} [(R^{(g+1)} / R^{(g)})^2]$. The quality gain is defined as the expected value $q_{\text{sph}} := \mathbb{E} [(R^{(g)})^2 - (R^{(g+1)})^2]$. By introducing the quality gain normalization $q_{\text{sph}}^* = q_{\text{sph}} N / (2R^2)$, see [12, p. 16], one has

$$\mathbb{E} \left[(R^{(g+1)} / R^{(g)})^2 \right] = 1 - 2q_{\text{sph}}^* / N. \quad (\text{A.28})$$

The expectation of the fourth order term in (A.27) cannot be easily evaluated, but it can be approximated. By

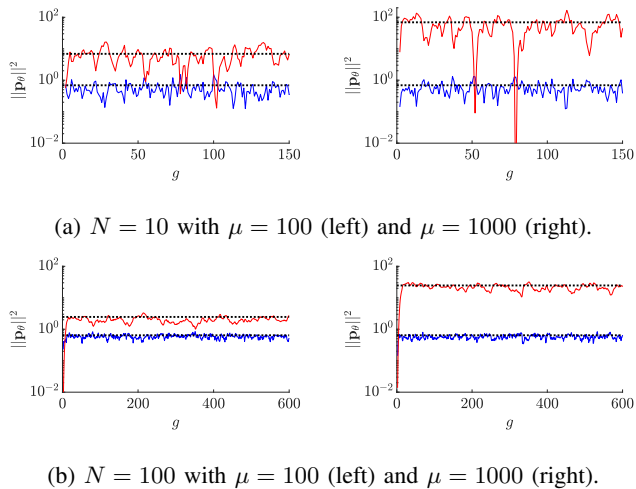


Fig. 11: PSA-CSA-ES at constant population size on the sphere, using CSA (15) and $\beta = 1/\sqrt{N}$. The blue signal shows $\|\mathbf{p}_m\|^2$ and the red signal $\|\mathbf{p}_c\|^2$, respectively (the sum $\|\mathbf{p}_\theta\|^2$ is not shown to improve visibility). The respective black horizontal lines show steady-state predictions $\|\mathbf{p}_m\|^2$ (A.21) and $\|\mathbf{p}_c\|^2$ (A.30), both evaluated at $\gamma = 0.88$ (see Fig. 2).

neglecting fluctuations of the quality gain, one demands $\text{Var}[x^2] = \text{E}[x^4] - \text{E}[x^2]^2 \stackrel{!}{=} 0$, $x = R^{(g+1)}/R^{(g)}$, such that $\text{E}[x^4] = \text{E}[x^2]^2$. Inserting (A.28) into (A.27) and using $\text{E}[(R^{(g+1)}/R^{(g)})^4] = \left(1 - 2q_{\text{sph}}^*/N\right)^2$, one gets

$$\begin{aligned} \text{E}[s^2] &\approx \text{E}\left[\left(1 - \frac{2q_{\text{sph}}^*}{N}\right)^2 - 2\left(1 - \frac{2q_{\text{sph}}^*}{N}\right) + 1\right] \\ &= \left(\frac{2}{N}q_{\text{sph}}^*\right)^2 \simeq \left(\frac{2}{N}\varphi^*\right)^2. \end{aligned} \quad (\text{A.29})$$

For the last (asymptotic) equality in (A.29), it was used that $\varphi^* \simeq q_{\text{sph}}^*$ holds for sufficiently large N , see [12, p. 16]. Since φ^* as a function of γ is known from (9), we are now in a position to insert the results back into (A.26). One gets

$$\begin{aligned} \|\mathbf{p}_c\|^2 &= \left(\frac{1}{\beta} - \frac{1}{2}\right)\mu \left(\frac{2}{N}\varphi^*\right)^2 \\ &= \left(\frac{1}{\beta} - \frac{1}{2}\right)\frac{8c_\theta^2\mu}{N}(1-\gamma^2)^2. \end{aligned} \quad (\text{A.30})$$

Result (A.30) is notable since it predicts a linear scaling $\|\mathbf{p}_c\|^2 \propto \mu$ (assuming γ independent of μ). Furthermore, the contribution of $\|\mathbf{p}_c\|^2$ vanishes for the slow adaptation limit $\gamma \rightarrow 1$, in which σ does not change in expectation.

Figure 11 shows steady-state experiments on the sphere to investigate the predictions of $\|\mathbf{p}_m\|^2$ (A.21) and $\|\mathbf{p}_c\|^2$ (A.30). The horizontal lines show good agreement with the measured signals. Visually, they do show minor deviations from the mean signal values. However, since approximations were applied, this was expected. Furthermore, the goal here is to illustrate basic scaling properties of the PSA-measure w.r.t. the population size. As expected, $\|\mathbf{p}_m\|^2 < 1$ in the sphere steady-state, which is in contrast to $\|\mathbf{p}_m\|^2 = 1$ during random selection (see also discussion below (29)).

Furthermore, one observes good agreement for the scaling $\|\mathbf{p}_c\|^2 \propto \mu$ as μ is increased (from left to right). This behavior is a crucial property of the PSA. For small $\|\mathbf{p}_\theta\|^2 < \mathcal{T}$ on the sphere, the PSA increases μ to increase the respective $\|\mathbf{p}_c\|^2$ -contribution. This usually happens for small initial μ , even though a population increase is not necessary on the sphere. Hence, the PSA controls μ to achieve the target value $\|\mathbf{p}_\theta\|^2 \approx \mathcal{T}$. This explains the relatively high μ_{med} -levels of the PSA on the sphere observed throughout Sec. V.

D. Additional Experiments: APOP

In this section, the effects of σ -rescaling on the performance measure P_f of the APOP are investigated. The experiments of Fig. 6 (bottom plot) indicate an issue of the APOP with active population control for $r_\sigma = \sqrt{\mu^{(g+1)}/\mu^{(g)}}$ and no waiting time (P1 from Table I). In this case, one observes large oscillations of $\mu^{(g)}$ on the sphere, occurring at larger N -values. The issue is further illustrated in Fig. 12. In the given example, the measure P_f shows a comparably large initial value of roughly $P_f \approx 0.5$. The value is comparably large since the initial population size is small at $\mu^{(0)} = 4$. This is not critical as small populations exhibit more fitness deterioration (see also discussion of Fig. 5, top plot). Since $\mathcal{T} = 0.2$, $P_f > \mathcal{T}$ triggers an increase of μ . While μ increases and $r_\sigma = 1$ (no σ -rescaling), the top plot indicates performance improvement and P_f drops, which is the expected behavior on the sphere. Small oscillations around $\mathcal{T} = 0.2$ are observed due to the controlling effect. In the bottom plot with σ -rescaling $r_\sigma = \sqrt{\mu^{(g+1)}/\mu^{(g)}}$, P_f increases further indicating worse performance, even though f -convergence (blue dash-dotted curve) can be observed. $P_f = 1$ at some point, indicating that only fitness deterioration (of the median difference) was measured. When μ remains large (and constant) over many generations, P_f decreases again and reaches its minimum value zero. The result are undesired large oscillations of μ on the sphere.

The observed oscillations are discussed in Fig. 13. To this end, the distributions of offspring \tilde{f} -values are shown together with their corresponding median over the selected values for two consecutive generations. The goal is to illustrate the effects of σ -rescaling. The first experiment at g serves as a reference. It is initialized randomly at $R^{(g)} = 1$ and $\sigma^{(g)} = \gamma\sigma_{\varphi_0}^*R^{(g)}/N \approx 0.42$ was chosen ($\gamma = 0.9$) to generate similar conditions as obtained during the dynamic simulation. Given the parameter configuration at g , the ES achieves positive progress using (1) with $\text{E}[R^{(g+1)}] = 0.98$. Hence, we choose $R^{(g+1)} = 0.98$ for the updated histogram. Since $P_f > \mathcal{T}$ is initially large in Fig. 12, a population size increase is triggered with $\alpha_\mu = 1.05$. Using (11), the σ -rescaling $\sigma^{(g+1)} = \sigma^{(g)}\sqrt{\alpha_\mu}$ is applied to simulate its effect on the APOP. The distribution of the \tilde{f} -values and the median change considerably. Despite having positive progress, the APOP indicates bad performance via $f_{\text{med}}^{(g+1)} - f_{\text{med}}^{(g)} > 0$ (minimization). Hence, the APOP collects information about the change in the distribution of \tilde{f} instead of the actual performance (note that progress rate and quality gain are asymptotically equal on the sphere [12, p. 16]). One observes

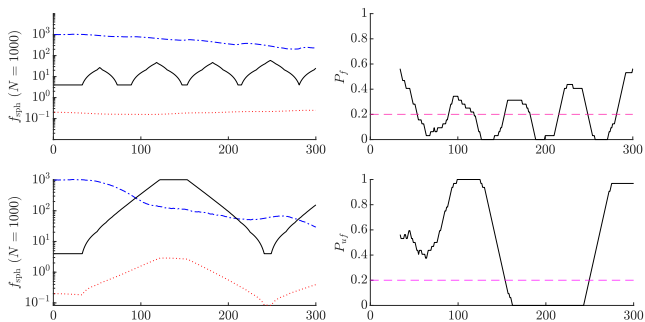


Fig. 12: APOP on the sphere ($N = 1000$) with $r_\sigma = 1$ (top) and $r_\sigma = \sqrt{\mu^{(g+1)}/\mu^{(g)}}$ (bottom), using (P1 from Tab. I).

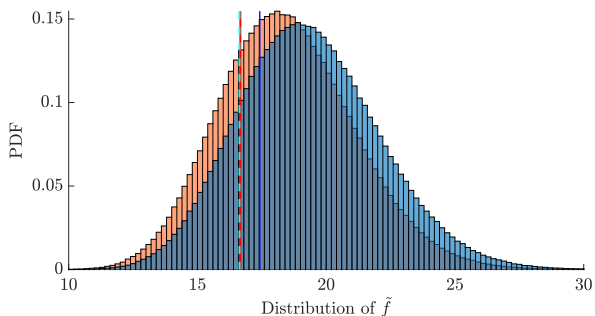


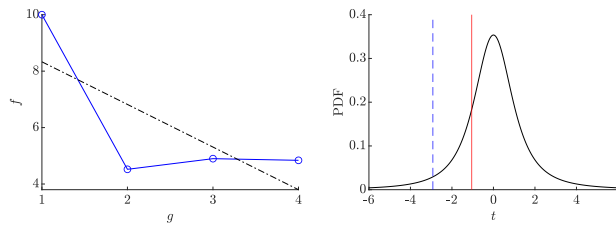
Fig. 13: Distribution change of offspring \tilde{f} -values on the sphere $N = 100$ over two generations g and $g + 1$. (100/100_I, 200)-ES is used with 10^4 repetitions. The reddish histogram shows $R^{(g)} = 1$ with $\sigma^{(g)} \approx 0.42$. The median over selected values (red vertical line, $\vartheta = 1/2$) yields 16.66. The blue histogram shows $R^{(g+1)} = 0.98$ and $\sigma^{(g+1)} = \sigma^{(g)} \sqrt{\alpha_\mu} \approx 0.43$ (rescaled using (11) with $\alpha_\mu = 1.05$) with median=17.42 (blue). For $R^{(g+1)} = 0.98$ with $\sigma^{(g+1)}$ not rescaled, the median yields 16.63 (cyan dashed, histogram not shown).

from the histograms that the quality gain expected value and variance change with varying σ . Note that if σ is not rescaled, i.e., $r_\sigma = 1$, the median at $g + 1$ decreases (slightly) compared to g , indicating good performance. Given this observation, the APOP should be evaluated with $r_\sigma = 1$ or a waiting time $\Delta_g > 0$ should be introduced. This is done by choosing P2 (from Tab. I), which improves the results and reduces the observed oscillations significantly.

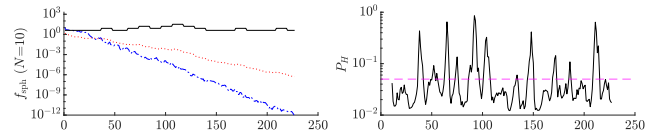
E. Additional Experiments: pcCSA

In this section, the failing of the convergence test of the pcCSA (see Fig. 7, bottom) is discussed, giving $P_H > 0.05$ consistently on the sphere function. This leads to an unnecessary increase of μ .

To this end, Fig. 14a illustrates the issue of the hypothesis test for a very small sample size $L = 4$. Note that this also occurs at (slightly) larger values of L . One observes a negative slope of f -values and the linear regression curve (left). The hypothesis test on the right side, however, indicates $P_H > 0.05$. Hence, it fails to reject the null hypothesis of



(a) Hypothesis test of pcCSA at $g = 4$ for the sphere at $N = 10$ and using $L = \lceil \sqrt{N} \rceil = 4$ (P1 from Tab. I). On the left, the f -values are shown as blue dots and the linear regression line in dash-dotted black. On the right, the corresponding t -distribution (solid black) is shown with $P_H > \alpha_H$ (P_H in red, threshold 0.05 in dashed blue).



(b) Dynamics with P2 from Tab. I using a sample size $L = 10$ for the hypothesis test.

Fig. 14: Analysis of pcCSA hypothesis test for small sample size L .

stagnation and the population is increased. At small L the standard error $s_{\hat{a}}$ attains comparably large values, see (26). In the case of large errors, the hypothesis test fails to reject H_0 and the decision is made towards larger populations, which is the more robust choice. The results improve significantly for $L = 10$ (P2) on the sphere $N = 10$ compared to P1, see ‘‘S10’’ in Tab. II for pcCSA. The dynamics of this example are shown in Fig. 14b.

F. Additional Experiments: PSA

Additional experiments of the PSA-CSA-ES are shown on the random function, investigating the influence of σ -rescaling and suboptimal performance observed in bottom plot of Fig. 8. The top plot in Fig. 15 shows the bottom plot of Fig. 8 as a reference. Removing the σ -rescaling ($r_\sigma = 1$ in center plot) does not improve the μ -levels on the random function. Instead, significantly better performance is obtained using CSA (17c) (bottom plot). The slower adaptation of σ (less fluctuations can be observed) yields a more stable signal of $\|\mathbf{p}_\theta\|^2$ (less fluctuations of $\|\mathbf{p}_c\|^2$), which in turns leads to better detection of random selection and higher μ -levels.

G. Additional Dynamics

Exemplary dynamics of the experiments from Fig. 9 are shown in Fig. 16. For APOP and pcCSA at $N = 10$, one observes good performance. The μ -levels (solid black) increase and remain high as local attraction is present (f -stagnation, dash-dotted blue). Within the global attractor, μ decreases again. For large $N = 1000$ the performance of APOP and (especially) pcCSA deteriorate. During the first phase of f -stagnation, one observes a notable increase of μ , which is desired. However, μ does not remain stable at high levels. On the right one observes that the performance measures P_f and P_H tend to oscillate around their thresholds. The

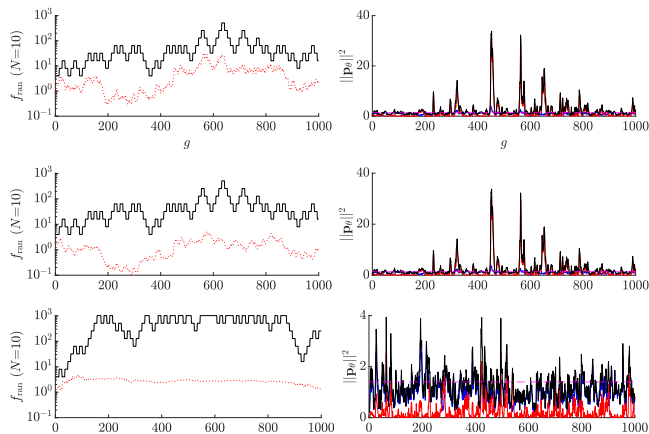


Fig. 15: PSA-dynamics with CSA (17a) (top, center) and CSA (17c) (bottom) for the random function $N = 10$ (P2 from Tab. I). Center and bottom plot use $r_\sigma = 1$ (no σ -rescaling).

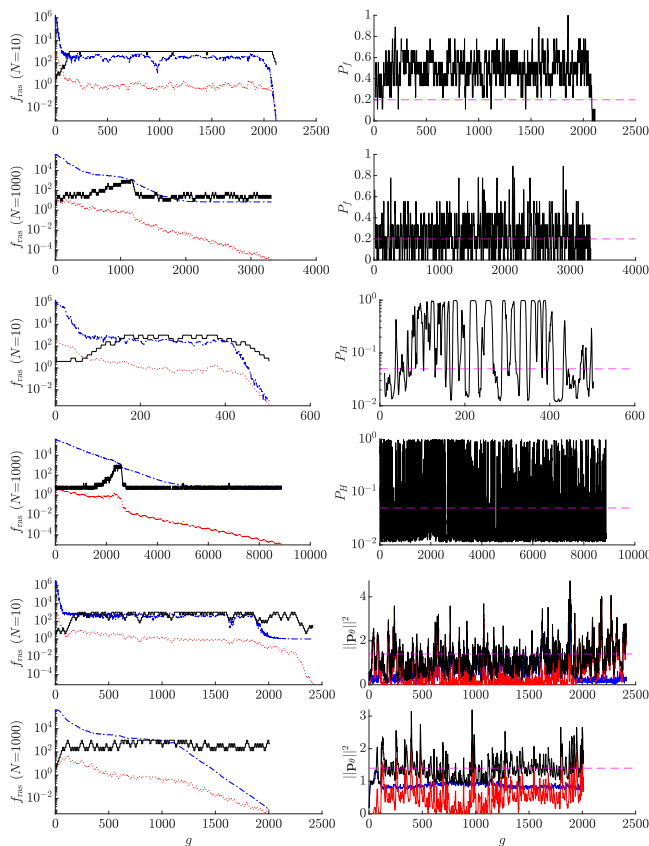


Fig. 16: Example runs from Fig. 9 for APOP, pcCSA, and PSA, from top to bottom, with each showing $N = 10$, $A = 65$ (top) and $N = 1000$, $A = 3$ (bottom), respectively (see y-axis labels).

PCS do not consistently detect insufficient performance as the ES progresses very slowly, but steadily due to exponentially many local attractors (in N). Hence, both APOP and pcCSA decrease μ too early (see left plots). The PSA on the other hand is more robust at large $N = 1000$, showing higher P_S . Its μ -levels tend to be comparably high, but its $\mu^{(g)}$ -dynamics

shows notable oscillations ($N = 1000$). However, note that its μ -levels in the sphere limits of Rastrigin (linear convergence of f) are also relatively high. At small $N = 10$, its performance drops to some extent due to larger influence of σ -fluctuations.